Central cholinergic regulation of the GnRH system: involvement of ACh/GABA co-transmission

Short title: **Cholinergic control of reproduction**

Csaba Vastagh[1¶*], Imre Farkas[1¶], Veronika Csillag[1], Masahiko Watanabe[2], Imre Kalló[1], Zsolt Liposits[1*]

[1]Laboratory of Endocrine Neurobiology, Institute of Experimental Medicine, Eötvös Loránd Research Network, Szigony u. 43, Budapest, H-1083, Hungary

[2]Department of Anatomy, Hokkaido University School of Medicine, Sapporo 060-8638, Japan.

[¶] These authors contributed equally to this work.

[*]Corresponding authors: vastagh.csaba@koki.hu and liposits.zsolt@koki.hu

Abstract

Gonadotropin-releasing hormone (GnRH)-synthesizing neurons orchestrate reproduction centrally. They receive commands from various neuronal networks for regulation of the hypothalamo-pituitary-gonadal (HPG)-axis. Here we report acetylcholine (ACh) as a critical regulator of GnRH neurons and reproduction in mice. In acute brain slice preparation, the acetylcholine receptor (AChR) agonists, ACh and carbachol, evoked a biphasic effect on the firing rate in GnRH neurons, first increasing afterwards diminishing it. In the presence of tetrodotoxin, carbachol induced an inward current followed by a decline in frequency of mPSCs. RT-PCR and whole cell patch-clamp studies revealed that GnRH neurons expressed both muscarinic (M1-M5) and nicotinic ($\alpha4\beta2$, $\alpha3\beta4$ and $\alpha7$) ACh receptors. Muscarine via M1 and M3 receptors increased, while via M2 and M4 reduced the frequency of both miniature postsynaptic currents (mPSCs) and firing. The identified nicotinic AChRs contributed to the nicotine-elicited inward current and the rise of firing rate. Optogenetic activation of channelrhodopsin-2-tagged cholinergic axons modified GnRH neuronal activity and evoked co-transmission of ACh and GABA from a subpopulation of boutons. 3DISCO immunocytochemistry and electron microscopy revealed innervation of GnRH neurons by cholinergic axons. Rabies retrograde viral labelling started from GnRH-Cre neurons identified the medial septum and the diagonal band of Broca as exclusive sites of origin for specific cholinergic afferents. *In vivo* pharmacogenetic activation of cholinergic system resulted in an increased secretion of luteinizing hormone (LH) in gonadectomized mice. Our findings collectively corroborate that the central cholinergic system exerts an important regulatory influence upon GnRH neurons and activates the HPG-axis via ACh and ACh/GABA neurotransmissions.

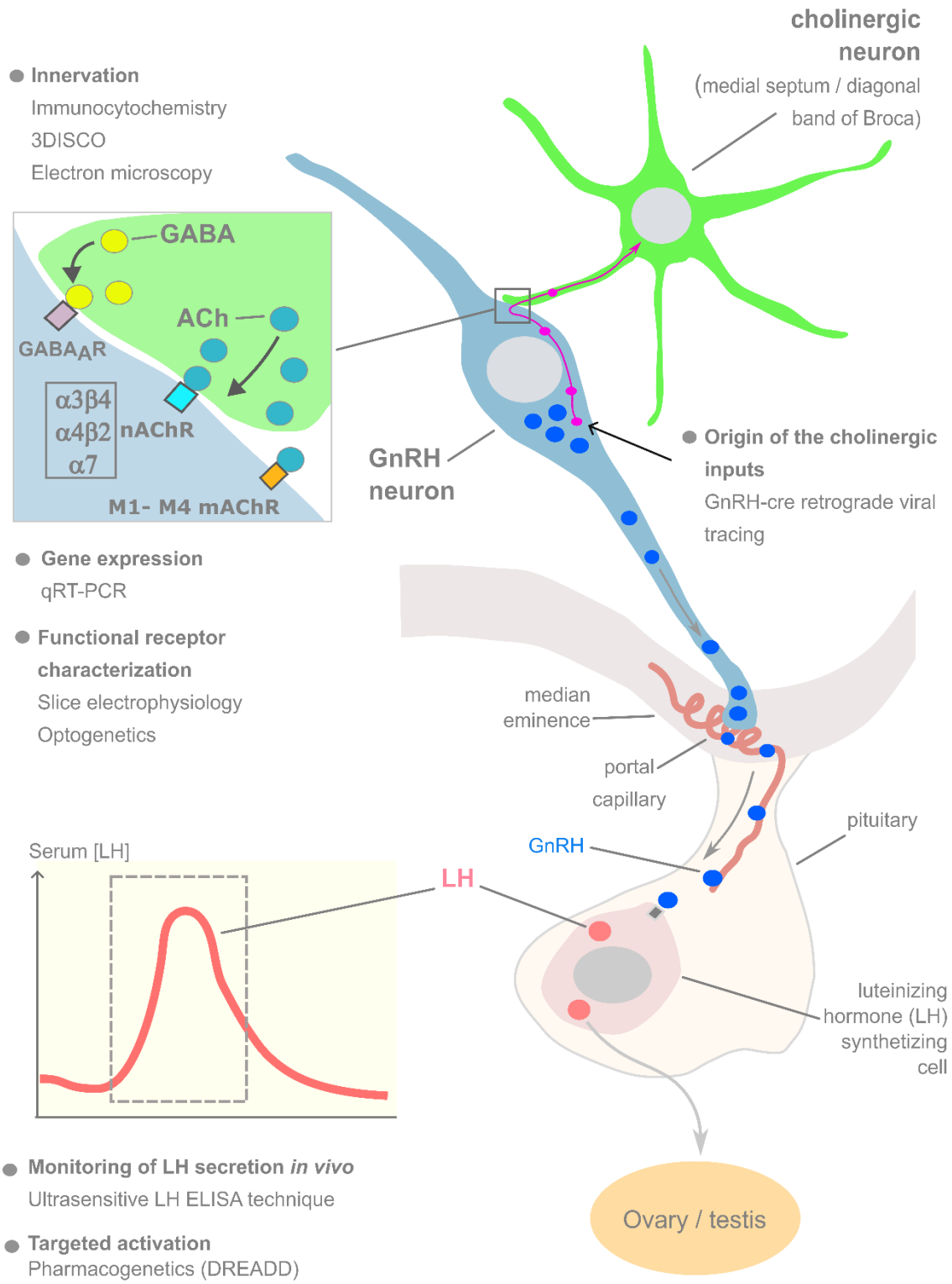

Graphical abstract

Abbreviations

AAV: adeno-associated virus
ACh: acetylcholine
Chat: choline acetyltransferase
ChR2: channelrhodopsin 2
CNO: clozapine N-oxide
Cono: α–conotoxin AuIB
Dari: darifenacin
DBB: diagonal band of Broca
DHBE: dihydro-β-erythroidine hydrobromide
DREADD: Designer Receptors Exclusively Activated by Designer Drug
ELISA: enzyme-linked immunosorbent assay
emPSC: evoked miniature postsynaptic current
G: G-protein
Gq: Gq protein alpha subunit
GFP: green fluorescent protein
GnRH: gonadotropin-releasing hormone
HPG: hypothalamo-pituitary-gonadal
ICC: immunocytochemistry
LH: luteinizing hormone
methoct: methoctramine
M: muscarinic receptor
mPOA: medial preoptic area
MS: medial septum
nAChR: nicotinic acetylcholine receptor
mAChR: muscarinic acetylcholine receptor
mPSC: miniature postsynaptic current
piren: pirenzepine
RJR: RJR2403
PNU: PNU282987
RV: rabies virus
THL: tetrahydrolipstatin
tropi: tropicamide
TVA: avian tumor virus receptor A
VAChT: vesicular acetylcholine transporter
VGAT: vesicular GABA transporter

Introduction

In vertebrates, the success of reproduction depends on the integrity of the hypothalamo-pituitary-gonadal (HPG) axis and the availability of the master molecule, gonadotropin-releasing hormone (GnRH) [1]. GnRH is synthesized in neurons of olfactory placode origin [2] which migrate through the basal forebrain and settle down at species-specific anatomical locations [3-5]. Via their hypophysiotropic axon projections, the cells secrete GnRH in a pulsatile manner into the hypophysial portal circulation [6] to control the proper gonadotroph hormone output of the anterior pituitary. The loosely organized GnRH cell population receives neuronal inputs from over fifty different brain regions [7], processes and integrates information on circulating gonadal hormones [8, 9] and a wide range of peripheral metabolic signals [10-13]. Failure of cell migration, disturbances in sensing and processing peripheral hormone signals or inability to respond properly to neurotransmitters/neuropeptides released from their synaptic afferents result in GnRH neuron and HPG axis dysfunctions or infertility [14, 15]. These pathological events interfere with the maintenance of species, therefore, the understanding of the diverse regulatory mechanisms of GnRH neurons at the molecular and cellular levels has been essential.

Most of the classic neurotransmitter systems, including glutamate [16] and GABA [17] have been shown to regulate reproduction centrally via synaptic channels onto GnRH neurons. Acetylcholine (ACh) is a highly potent neurotransmitter used widely for communication in both the central and peripheral nervous systems. Its effects are executed via nicotinic [18] and muscarinic ACh receptor [19] subtypes that are differentially expressed in diverse neuron phenotypes. Cholinergic signaling has been proposed to control reproduction centrally. Early *in vivo* studies have shown that nicotine delays the surge release of luteinizing hormone (LH) [20], inhibits the progesterone-advanced LH surge in proestrus [21], blocks the LH secretion induced by opioid receptor antagonist [22] and decreases the pulsatile secretion of LH [23]. Under *in vitro* conditions the natural ligand, ACh stimulated the release of GnRH from hypothalamic fragments and the secretion of LH [24]. The involvement of muscarinic mechanisms has also been shown since selective muscarine receptor antagonists stimulated the release of GnRH from the median eminence of the rat [25]. The use of immortalized GnRH neurons (GT1-7 cells) allowed the characterization of some molecular mechanisms involved in the cholinergic modulation of GnRH neurons. These cells express functional high

affinity α4β2 and α7 subtypes of nicotinic ACh receptors (nAChR) and the activation of the α-bungarotoxin sensitive α7 subclass by nicotine exerts inhibitory effect on GnRH release [26]. A biphasic action of ACh on GnRH release was seen in perifused hypothalamic cells and GT1-7 neurons, whereas nicotine alone increased and muscarine decreased the release of the neurohormone [27]. While nicotinic and muscarinic M1 receptors exert stimulatory effects, activation of muscarinic M2 receptors inhibits GnRH release [27]. Transcriptome profiling of rodent GnRH neurons and GT1-7 cells has confirmed the expression of certain nicotinic and muscarinic receptors [28-30] supporting the view of a direct action of cholinergic drugs upon GnRH neurons. It has been shown recently that murine GnRH neurons grown in nasal explants receive regulatory acetylcholine neurotransmission [31]. Although these findings unequivocally imply that the central cholinergic system modulates the operation GnRH neurons, the precise anatomical background of networking between the cholinergic and GnRH systems, the exact origin(s) of cholinergic inputs and the responses of GnRH cells to different ACh receptor subtype specific ligands are still in obscurity in adult mice.

Therefore, the present study was undertaken to (1) explore the putative networking of the central cholinergic system with hypophysiotropic GnRH neurons, (2) elucidate the source(s) of ACh involved in neurotransmission, (3) reveal the type(s) of cholinergic receptors expressed in GnRH neurons, (4) characterize the effects of ACh receptor ligands on function of GnRH cells and (5) measure the impact of *in vivo* chemogenetic activation of cholinergic neurons on luteinizing hormone secretion in adult mice.

Results

Cholinergic drugs change the electrophysiological activity of GnRH neurons in acute brain slice

Carbachol triggers ion current and modifies mPSCs of GnRH cells

We studied the effects of activation of nicotinic and muscarinic AChRs by the AChR agonist, carbachol on the membrane current and miniature postsynaptic currents (mPSCs) in voltage-clamp mode at -70 mV. Application of carbachol in a single bolus triggered a transient inward current (amplitude = -36.9 ± 3.09 pA, Student's t-test: N/n=3/9, p=0.0001, t=11.95, df=8; duration = 47.9 ± 12.34 s) (**Fig 1a**). Thereafter, the frequency of mPSCs significantly decreased (65.7 ± 6.01 % of the control value, **Fig 1a**). We hypothesized that the inward current is caused by nAChR. Therefore, we next pretreated the brain slices with mecamylamine (non-selective nAChR antagonist,10 μM), and then carbachol was added to the aCSF (**Fig 1b**). Disappearance of the inward current confirmed that nAChR activation is involved in the effect of carbachol on membrane current. Nevertheless, the significant decrease in the frequency of the mPSCs was still observable (57.2 ± 6.88 % of the control value, (**Fig 1b**) raising the possibility that mAChRs play a role in the regulation of mPSC frequencies. Thus, next the slices were pretreated with a cocktail of mecamylamine (10 μM) and the non-selective mAChR antagonist, atropine (10 μM), and then carbachol was added to the aCSF (**Fig 1c**). The inward current disappeared and the frequency of mPSCs remained unchanged in this experiment (frequency: 97.2 ± 3.41 % of the control value, **Fig 1c**).

To confirm the regulatory role of mAChRs in the decrease in the frequency of mPSCs, in the next experiment the mAChR agonist muscarine (100 μM) was added to the aCSF in a single bolus. The measurements revealed that no inward current was evoked by muscarine. Nevertheless, a significant decrease in the frequency of mPSCs was detected (68.1 ± 6.67 % of the control value, **Fig 1d**). However, atropine pretreatment abolished this change in the frequency (103.5 ± 5.11 % of the control value, **Fig, 1e**). These results of the frequency changes are summarized in the bar graph (**Fig 1f**) showing that mAChRs play a pivotal role in the decrease of frequency of mPSCs.

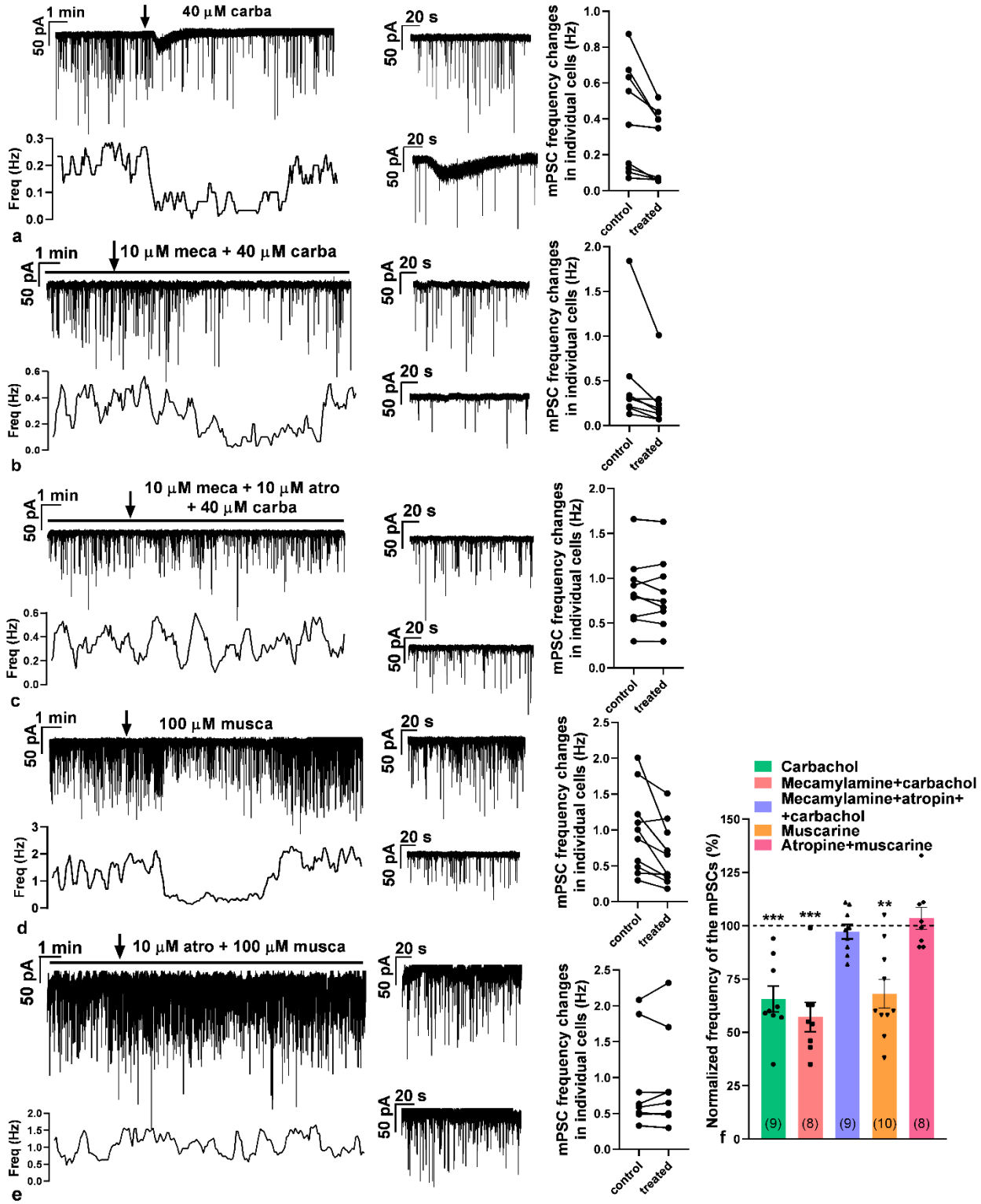

Fig 1. **Effect of carbachol on the membrane current and mPSCs of GnRH neurons**. Representative recordings illustrate that carbachol (40 μM) first evoked an inward current and then an inhibitory action on mPSCs of GnRH neurons in the presence of tetrodotoxin (660 nM). **a**. Carbachol triggered an inward current followed by a slower inhibitory effect on the frequency of mPSCs. **b**. Mecamylamine pretreatment (10 μM) revealed that the inward current is related to

nicotinic receptors. **c**. Simultaneous pretreatment with mecamylamine and atropine (10 μM) eliminated both the inward current and the inhibitory effect of carbachol. **d**. Muscarine 100 μM) evoked exclusively the inhibitory effect upon mPSCs. **e**. This inhibitory effect was totally abolished by atropine pretreatment. **f.** The bar graph summarizes the results detailed above (numbers of measured neurons are in parenthesis). **=p<0.01, ***=p<0.005. Horizontal black lines above the recordings show the presence of various AChR receptor subtype specific inhibitors (mecamylamine, atropine) in the aCSF. The arrow shows the time of administration of carbachol or muscarine. Zoomed 2.5 min long recordings of control (upper graph) and treated (lower graph) periods are besides the recordings. Changes in the frequency of mPSCs of individual GnRH neurons are shown besides these zoomed recordings. Frequency distribution of the mPSCs is graphed under each recording. carba=carbachol, atro=atropine, musca=muscarine, meca=mecamylamine.

ACh and carbachol change the firing of GnRH neurons

Postsynaptic currents and firing activity of GnRH neurons positively correlate with each other [32, 33]. To evaluate therefore the effect of acetylcholine (ACh) on the electric activity of GnRH neurons, firing was recorded in whole-cell current clamp mode. A single bolus of ACh (50 μM), the natural ligand of the cholinergic system, evoked a biphasic change in the firing rate (**Fig 2a**). An initial stimulatory phase was followed by a robust inhibitory phase. Thorough examination of the recording, however, revealed that the stimulatory phase can be further divided into two subphases (phase I =0.5 min, phase II =3 min), while no subphases could be defined in the inhibitory phase (phase III =3 min). The length of these phases were defined by an approximate estimation and did not take into consideration the accidental overlaps. The firing rate changed significantly in all three phases (**Fig 2a,** phase I: 409.3 ± 49.44%, phase II: 285.3 ± 39.91%, phase III: 44.6 ± 8.93%, washout: 98.7 ± 10.18% of the control firing rate).

We also studied the effects of carbachol (a widely used AChR agonist not metabolized by ACh-esterase) administration (40 μM) on the firing rate of GnRH neurons (**Fig 2b**). The phases of the evoked effects mimicked those of ACh and showed significant changes in the firing rate (**Fig 2b,** phase I: 186.9 ±

20.47%, phase II: 140.4 ± 9.23%, phase III: 28.6 ± 7.486%, washout: 105.1 ± 6.27% of the control firing rate [the data before agonist application]).

To elucidate the nature of AChRs involved in the observed effect, the brain slices were pretreated with mecamylamine (10 μM) then carbachol was applied. Carbachol application first accelerated then inhibited the firing activity of GnRH neurons (**Fig 2c**). Examination of the recordings, however, clearly showed that phase I. was absent, whereas phase II. was present in the stimulatory phase, showing that functional nAChRs play role in phase I. Statistical analysis revealed that phase II and phase III represented significant changes in the firing rate (**Fig 2c,** phase I: 99.4 ± 3.311%, phase II: 156. 9 ± 12.16%, phase III: 37.7 ± 7.67%, washout: 103.4 ± 5.29% of the control firing rate), suggesting that mAChRs also take part in the cholinergic control of GnRH neuron firing.

To confirm the contribution of mAChRs to the control of GnRH neuron firing, the brain slices were pretreated with atropine (10 μM), and then carbachol was added in a single bolus to the aCSF in the measuring chamber. The recordings showed that carbachol induced a short stimulatory phase, but no subsequent inhibition occurred in the presence of atropine (**Fig 2d**). The short stimulation resembled phase I. In contrast, phases II and III were absent (**Fig 2d,** phase I: 179.3 ± 12.6%, phase II: 104.5 ± 4.95%, phase III: 94.9 ± 6.485%, washout: 102.9 ± 3.912% of the control firing rate).

Altogether, these results show that nAChRs control phase I of the evoked firing, while phases II and III are regulated by stimulatory and inhibitory subtypes of mAChRs, respectively.

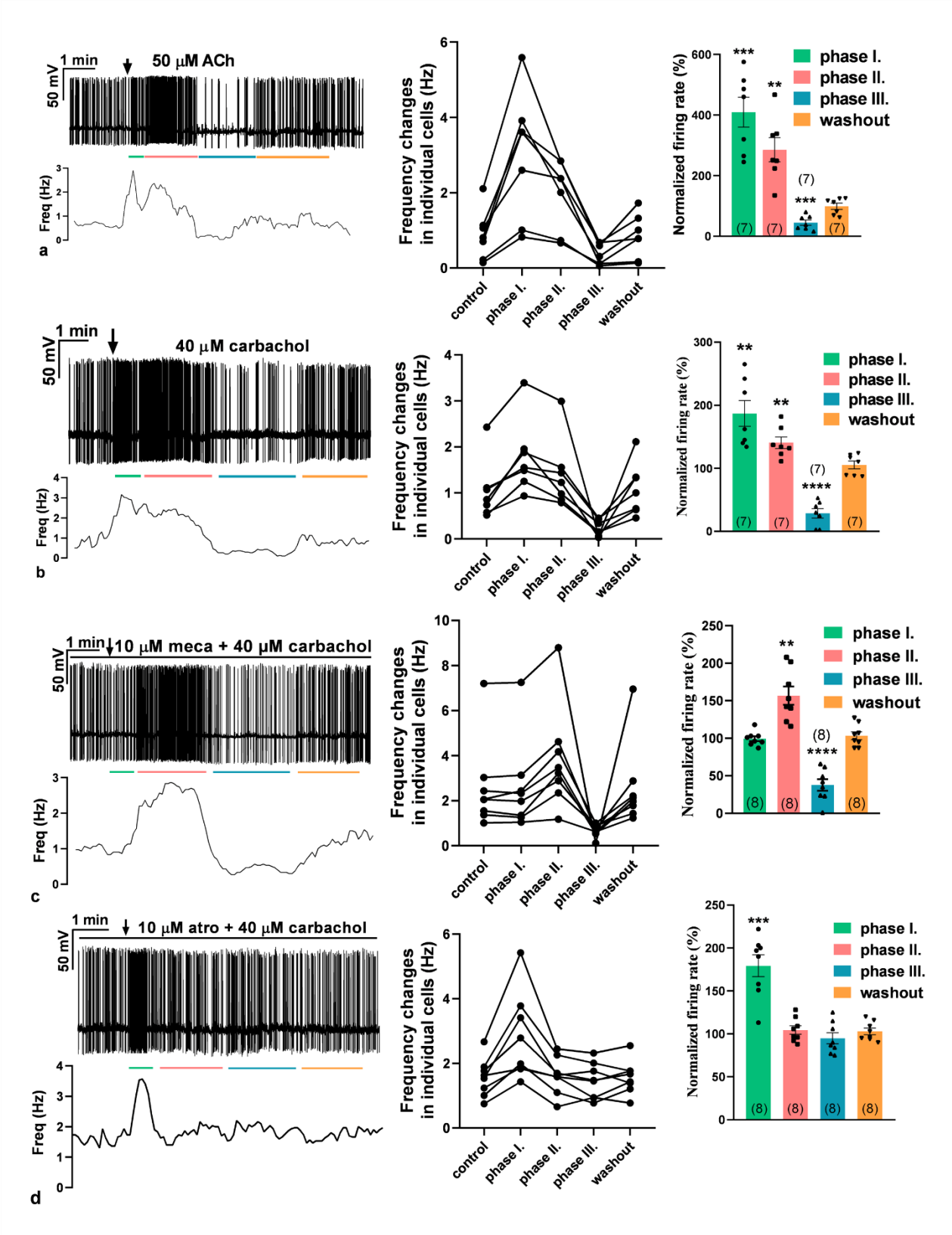

198

199 **Fig 2**. **Effect of acetylcholine and carbachol on firing rate of GnRH neurons. a**. ACh (50 μM)
200 evoked a biphasic action. First it increased, then robustly inhibited the firing rate. **b**. Carbachol (40
201 μM) also triggered a biphasic effect with a first elevation followed by a later decline in the firing
202 rate. **c**. Mecamylamine (10 μM, nicotinic acetylcholine receptor antagonist) pretreatment
203 eliminated the first, 0.5 min part of the elevation phase suggesting that the facilitatory phase can

be further divided into two subphases standing for nicotinic (phase I) and muscarinic (phase II) stimulatory actions, respectively. **d.** Atropine (10 μM) pretreatment abolished both phase II of facilitation and the inhibitory phase (phase III) proving that these phases stand for muscarinic effects. Arrow shows the time of administration of ACh or carbachol. The horizontal black line above the recordings indicates the presence of inhibitors (mecamylamine or atropine). Changes in the firing rate of individual GnRH neurons and the percentage changes are shown besides each recording. Frequency distribution of firing rate is graphed under each recording. Phase I=0.5 min, phase II=3 min, phase III=3 min. The colored lines under the recordings match the colors of the bar graphs and represent the various phases. **=p<0.01, ***=p<0.005, ****=p<0.001. Meca=mecamylamine, atro=atropine. Numbers of the measured neurons are in parenthesis.

Hypophysiotropic GnRH neurons express various nicotinic and muscarinic ACh receptors

Cytoplasmic samples (n = 70) were collected from GnRH-GFP neurons by patch pipette aspiration, sorted into separate cytoplasmic sample pools (CPs, n = 7) and examined by quantitative real-time PCR (qRT-PCR). The primer probe sets used for detection of expression of genes encoding for muscarinic and nicotinic ACh receptors, housekeeping genes (*Hprt*, *Gapdh*) and *Gnrh1* are summarized in **S1 Table**. Examination of the sample groups revealed the relative mRNA expression level of genes encoding for the following nicotinic receptor subunits in GnRH neurons (mean ± SE, **Fig 3b**): alpha 3 subunit (*Chrna*3) 0.026 ± 0.006 (detected in 2 of 7 CPs), alpha 4 subunit (*Chrna4*) 0.016 ± 0.009 (2 of 7 CPs), alpha 7 subunit (*Chrna7*) 0.018 ± 0.009 (3 of 7 CPs), beta 2 subunit (*Chrnb2*) 0.015 ± 0.005 (4 of 7 CPs); beta 3 subunit (*Chrnb3*) 0.023 ± 0.11 (4 of 7 CPs) and beta 4 subunit (*Chrnb4*) 0.047 ± 0.016 (5-of 7 CPs). Regarding muscarinic receptors (M1 – M5), muscarinic type 1 (*Chrm1*) 0.034 ± 0.004 (5 of 7 CPs), type 2 (*Chrm2*) 0.011 ± 0.006 (2 of 7 CPs), type 3 (*Chrm3*) 0.048 ± 0.016 (5 of 7 CPs), type 4 (*Chrm4*) 0.038 ± 0.013 (4 of 7 CPs) and type 5 (*Chrm5*) 0.037 ± 0.024 (3 of 7 CPs) receptor genes were also measured in the samples (**Fig 3b**.) The expression of *Gnrh* gene (30.2 ± 4.68) was confirmed in all samples (**Fig 3a)**.

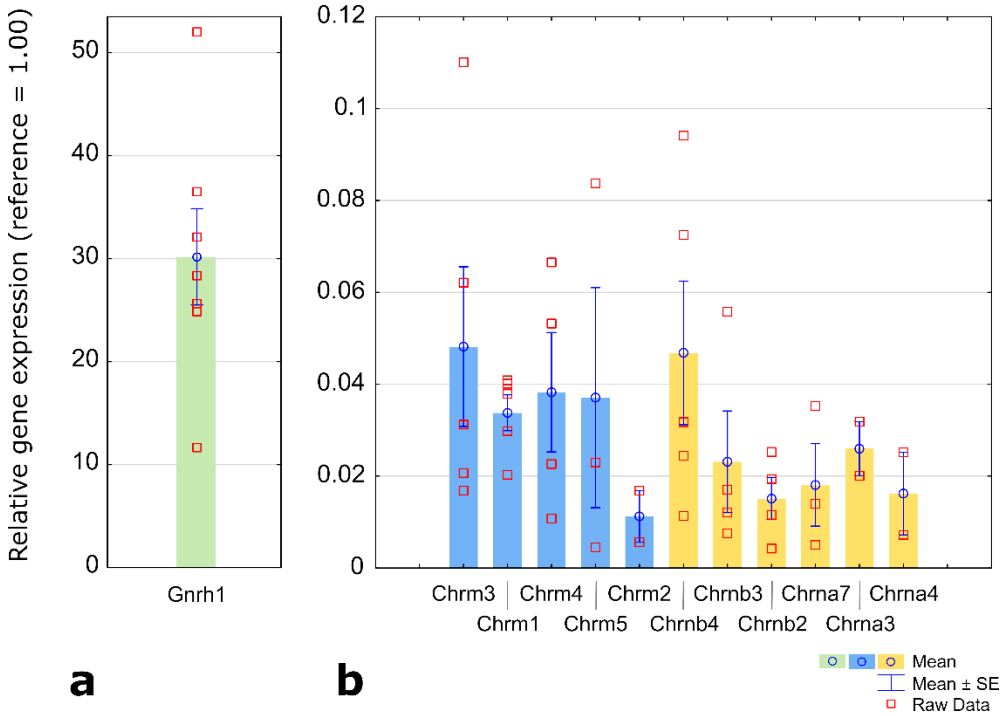

Fig 3. Expression of nicotinic and muscarinic ACh receptor genes in GnRH neurons. Relative expression of Gnrh1 gene (**a**) and various nicotine and muscarine acetylcholine receptor genes (**b**) in cytoplasmic sample pools of GnRH neurons revealed by qRT-PCR. The mean ± standard error of gene expression data is shown for each subunit as a proportion of the mean of the two reference genes.

Electrophysiological characterization of functional nicotinic receptor subtypes involved in the control of GnRH neurons

The qRT-PCR study revealed the expression of genes encoding various subunits of nAChR in GnRH neurons. Whole-cell voltage clamp measurements were carried out to identify the functional subtypes of nAChR involved in the control of GnRH neurons. Application of nicotine (10 µM, broadband agonist of nAChRs) triggered a robust inward current (amplitude = -41.5 ± 9.05 pA, duration = 58.9 ± 18.3 s, **Fig 4a and 4d**). One minute after the inward current has decayed, nicotine was applied again. Amplitude and duration of the second response to nicotine were the same as to its first application indicating that desensitization does not occur at this time scale (not shown). Then the slice was pretreated with DHBE (1 µM, antagonist of the α4β2 nAChR) and nicotine was applied again to the same neuron. An inward current was evoked again; however, its amplitude was significantly lower compared to the one observed when nicotine was added alone (amplitude = -18.4 ± 3.41 pA, duration = 84.4 ± 33.41 s, **Fig 4b and 4d**), indicating

that the α4β2 subtype of nAChR plays role in the observed effect. Next, α-conotoxin AuIB (1 μM, antagonist of α3β4 nAChR) was added to the aCSF containing DHBE and nicotine was administered again to the same neuron. This inhibitor cocktail significantly decreased further the amplitude (amplitude = -9.2 ± 2.36 pA, duration = 78.2 ± 38.6 s, **Fig 4c and 4d**), although it did not abolish the response completely. This suggests that GnRH neurons that express the α4β2 subtype also present the α3β4 subtype of nAChR.

To confirm this co-expression further, we next examined whether GnRH neurons expressing the α3β4 nAChR subtype also express the α4β2 subtype. Therefore, after measuring the nicotine-evoked inward current (amplitude = -42.9 ± 7.89 pA, duration = 68.7 ± 21.3 s, **Fig 4e and 4h**), then α-conotoxin AuIB was first added to the aCSF, and the nicotinic response was recorded again in the same neuron. Conotoxin pretreatment significantly decreased but did not eliminate the amplitude of the inward current (amplitude = -19.2 ± 2.83 pA, duration = 74.1 ± 28.39 s, **Fig 4f and 4h**), showing expression of the functional α3β4 type receptor. Then DHBE was also added to the aCSF. This cocktail significantly lowered the amplitude further but did not abolish the evoked response (amplitude = -9.2 ± 1.74 pA, duration = 71.1 ± 26.98 s, **Fig 4g and 4h**).

To present further evidence that the α4β2 subtype of nAChR is expressed in GnRH neurons, RJR2403 (100 μM, selective agonist of the α4β2 receptor) was applied in a single bolus. Application of RJR2403 evoked an inward current (amplitude = -22.9 ± 4.15 pA, duration = 98.9 ± 38.15 s, **Fig 4i and 4l**), which was abolished completely by DHBE pretreatment (amplitude = -1.2 ± 1.23 pA, **Fig 4j and 4l**). Because simultaneous blockade of α4β2 and α3β4 subtypes of nAChR did not eliminate completely the nicotine-evoked response in GnRH neurons, the participation of further nicotinic receptor(s) seemed reasonable in the regulatory process. We challenged the putative expression of the α7 subtype of the receptor. Therefore, PNU282987 (100 μM, selective agonist of the α7 subunits) was applied into the bath in a single bolus. It evoked a low amplitude, but still significant inward current (amplitude = -11.2 ± 1.88 pA, duration = 88.6 ± 25.15 s, **Fig 4k and 4l**). This finding indicates that the α7 subtype of nAChR also contributes to regulation of GnRH neurons, in addition to the α4β2 and the α3β4 receptor subtypes.

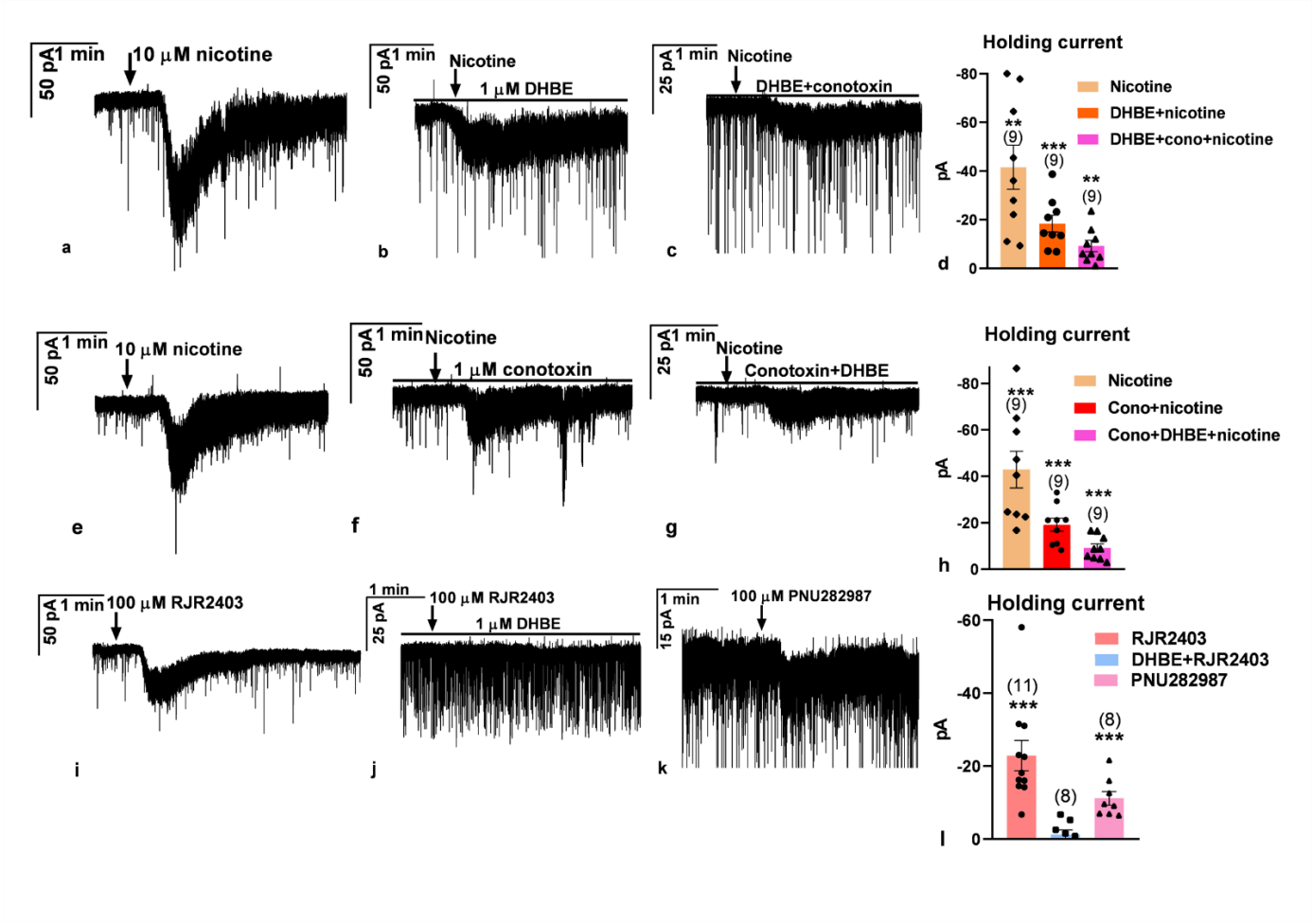

Fig 4. Characterization of functional nicotinic ACh receptors in GnRH neurons. Representative whole-cell patch voltage clamp recordings demonstrate that nicotine evokes an inward current in GnRH neurons, depending on the specific type of the ionotropic AChR. **a.** Nicotine administration (10 μM) induced a robust inward current. **b.** The α4β2 nAChR antagonist, DHBE (1 μM) significantly reduced the nicotine-evoked inward current measured in the same neuron as in **a** and **c**. The co-application of α3β4 antagonist, conotoxin (1 μM) with DHBE dampened the nicotine-evoked inward current further but did not eliminate it. The recording was carried out in the same neuron as in **a** and **b** showing that neurons expressing α4β2 receptor also present α3β4 receptor in their membrane. **d.** The bar graph summarizes the significant inward currents measured. **e.** In another neuron, nicotine also induced a strong inward current. **f.** The α3β4 receptor antagonist, conotoxin (1 μM) significantly reduced the evoked inward current measured in the same neuron as in **e** and **g**. Co-administration of DHBE attenuated the inward current further but did not abolish it. The recording was measured in the same neuron as in **e** and **f** showing that neurons expressing the α3β4 receptor also have functional α4β2 receptor in their membrane. **h**. The bar graph

summarizes these results. **i-j.** The α4β2 receptor agonist, RJR2403 (100 μM) also triggered an inward current which was abolished by DHBE pretreatment. **k**. The α7 subtype nAChR agonist, PNU282987 (100 μM) also evoked a low-amplitude inward current. **l.** The bar graph summarizes these results. DHBE=dihydro-β-erythroidine (α4β2 antagonist), conotoxin=α-conotoxin AuIB (α3β4 antagonist), RJR2403 (α4β2 agonist), PNU282987 (α7 agonist). Arrow shows the time of administration of various drugs. *=p<0.05, **<0.01, ***=p<0.005. The recordings in **a-b-c** were carried out in the first slice and the recordings in **e-g-f** were carried out in another slice.

Characterization of muscarinic receptor subtypes controlling GnRH neuron activity

Regulation of mPSC frequencies

Using whole-cell voltage clamp recordings, we examined the contribution of stimulatory (M1, M3) and inhibitory (M2, M4) muscarinic receptors to the regulation of mPSC frequencies in GnRH neurons. We have to note, that mPSCs are exclusively GABAergic [34] and GABA is excitatory via $GABA_A$-R due to the high intracellular chloride concentration in GnRH neurons of male mice [35]. Following a 1-min-long control registration period, blockade of the inhibitory receptors was carried out with a cocktail consisting of the M2 and M4 muscarinic receptor inhibitors, tropicamide and methoctramine, respectively. The treatment significantly increased the frequency of the mPSCs, suggesting a tonic release of ACh (127.3 ± 8.50% of the control value, **Fig 5a and 5e**). Then, muscarine (100 μM) was added in a single bolus into the measuring chamber in the continuous presence of the blocker cocktail. Muscarine significantly increased the frequency further (139.1 ± 14.75% of the pre-treatment value, **Fig 5a and 5f**). In the second step, the M1 and M3 stimulatory receptors were antagonized with a cocktail of darifenacin and pirenzepine, inhibitors of the M1 and M3 muscarinic receptors, respectively, and the measurements were carried out again. Blockade of the stimulatory muscarinic receptors decreased the frequency of the mPSCs significantly, confirming the tonic release of ACh (80.7 ± 2.67% of the control value, **Fig 5b and 5e**). Muscarine administration significantly diminished the frequency further (139.1 ± 14.75% of the pre-treatment value, **Fig 5b and 5f**).

Our earlier studies revealed that activation of retrograde 2-AG endocannabinoid signaling pathways can change the frequency of mPSCs in GnRH neurons. Therefore, tetrahydrolipstatin (THL), an inhibitor of

the 2-AG endocannabinoid production, was applied intracellularly in the patch pipette solution. Under this condition, cocktail of tropicamide+methoctramine evoked no notable change in the frequency of the mPSCs (102.2 ± 4.1% of the control value, **Fig 5c and 5e**), and muscarine application triggered no observable change either (106.5 ± 4.17% of the control value, **Fig 5c and 5f)**. Similarly, cocktail of darifenacin+pirenzepine resulted in no notable change in the frequency in the intracellular presence of THL (102.3 ± 5.1% of the control value, **Fig 5d and 5e)** and muscarine induced no significant alteration of the frequency either (106.4 ± 4.97% of the control value, **Fig 5d and 5f**). These data unveil the regulatory role of retrograde 2-AG endocannabinoid signaling in modulation of GnRH neuron physiology via both inhibitory and stimulatory types of muscarinic receptors.

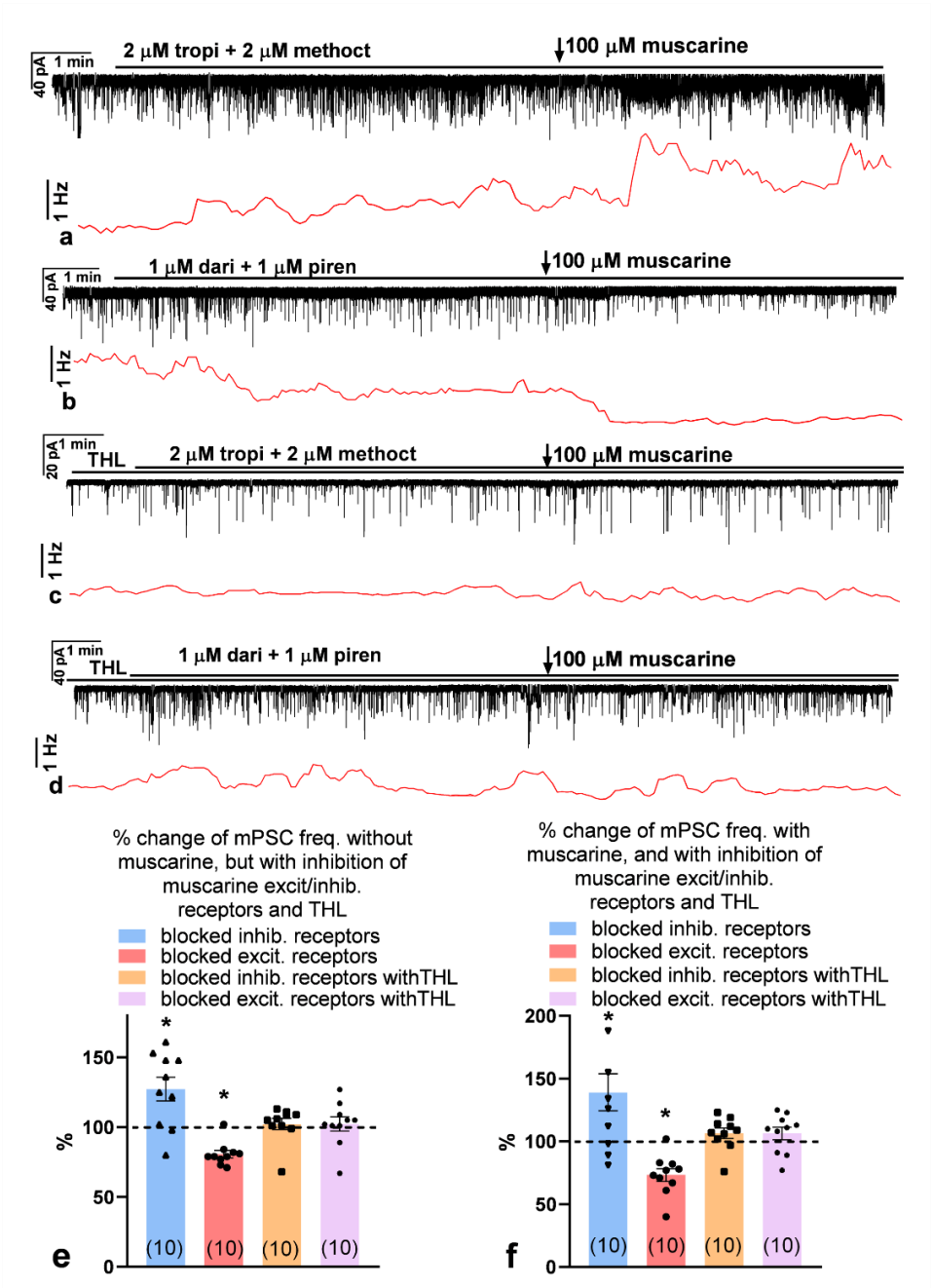

Fig 5. Functional characterization of muscarinic ACh receptors in GnRH neurons. Representative recordings prove effect of blockade of inhibitory (tropicamide+methoctramine) or stimulatory (darifenacin+pirenzepine) muscarinic receptors and muscarine on mPSCs in GnRH neurons in the intracellular absence/presence of THL, an inhibitor of retrograde 2-AG endocannabinoid signaling pathway. **a.** Blockade of inhibitory receptors increased frequency of mPSCs. Application of muscarine elevated the frequency further. **b.** Conversely, blockade of stimulatory receptors diminished frequency of mPSCs, and muscarine reduced it further. **c-d.** Intracellular presence of THL, however, abolished the effects, neither blockade of inhibitory/stimulatory receptors, nor application of muscarine evoked any significant action on the frequency. **e-f.** The bar graphs summarize these significant actions (numbers of measured neurons are in parenthesis). Horizontal black lines above the recordings show presence of various inhibitors (THL, dari=darifenacin [M3 inhibitor], methoct=methoctramine [M2 inhibitor], piren=pirenzepine [M1 inhibitor], tropi=tropicamide [M4 inhibitor]) and arrow points time of muscarine administration). *=$p<0.05$. Frequency distribution graphs are found under each recording.

Muscarine exerts a biphasic effect on firing of GnRH neurons

Our results suggested that besides the nACh-Rs functional mACh-R subtypes also exist in GnRH neurons. Therefore, the putative effects of the M1-M4 receptor forms on the firing activity of GnRH neurons were studied using whole-cell current clamp method. When muscarine (100 μM, broad-band agonist of mAChRs) was administered in a single bolus it evoked a biphasic effect. In the first 3 min period (phase I.) muscarine significantly elevated the firing rate (147.6 ± 10.28 % of the control firing rate, **Fig 6a**). In the second 3 min period (phase II) a significant decrease was seen in the firing rate (54.5 ± 6.9 % of the control firing rate, **Fig 6a**). To dissect further the phenomenon, first, we examined the function of M4 by pretreating the brain slices with tropicamide (2 μM, selective inhibitor of the M4 subtype of mACh-R then muscarine was administered. The recording clearly showed that both the stimulatory and the inhibitory phases developed (**Fig 6b**). The firing rate significantly increased up to 152 ± 14.8 % of the control value and then significantly decreased to 78.3 ± 5.53 % of it. However, phase II represented a decrease that was milder than

without tropicamide, suggesting that beside M4 another inhibitory subtype is involved. Next M2 was blocked by adding methoctramine (2 μM, selective inhibitor of the M2 subtype of mACh-R), then muscarine was applied. The stimulatory phase I. persisted in the presence of methoctramine revealing a significant increase in the firing rate (145.6 ± 6.59 % of the control value, **Fig 6c**). The inhibitory phase II. was also present because the firing rate significantly diminished (80.8 ± 3.45 % of the control value, **Fig 6c**). Phase II., however, displayed a smaller decrease than in the absence of the M2 or M4 antagonists, revealing role of the M2 subtype.

Next, we antagonized both inhibitory subtypes. In the presence of a cocktail of tropicamide and methoctramine, the stimulatory phase I. still existed (150.8 ± 12.61% of the control firing rate), but no inhibitory phase II. developed, rather a stimulation was seen in phase II. period (122.4 ± 8.76% of the control value) (**Fig 6d**). The changes in both phases were significant. The stimulatory period, therefore, lasted much longer in the presence of the M2 and M4 antagonists.

We also examined the function of the stimulatory mACh-R subtypes, M1 and M3. First pirenzepine (1 μM, selective antagonist of the M1 subtype of mACh-R) was added to the cocktail of tropicamide and methoctramine and then muscarine was applied. In the presence of these three antagonists, muscarine significantly increased firing rate in phase I. (118.9 ± 4.5% of the control firing rate, **Fig 6e**). Nevertheless, the value of the increase was lower than without pirenzepine, showing role of M1 in the stimulation. Phase II., however, presented no significant change at all (102.4 ± 6.42% of the control value). Thus, duration of the stimulation was not longer than three minutes.

Role of M3, the other stimulatory mACh-R subtype was also investigated. Darifenacin (1 μM, selective antagonist of the M3 subtype of mACh-Rs) was added to the cocktail of tropicamide and methoctramine and then muscarine was applied. Phase I. presented a significant elevation in the firing rate (119.4 ± 4.18% of the control firing rate, **Fig 6f**. Phase II. also displayed a significant increase in the firing rate (124.0 ± 9.71% of the control value, **Fig 6f,** thus the stimulation lasted much longer than three minutes.

Finally, the effect of muscarine was examined in the presence of M1-M2-M3-M4 antagonists. This cocktail abolished both phase I. (105.3 ± 8.31% of the control value) and phase II. (103.2 ± 7.89% of the control firing rate) completely (**Fig 6g**).

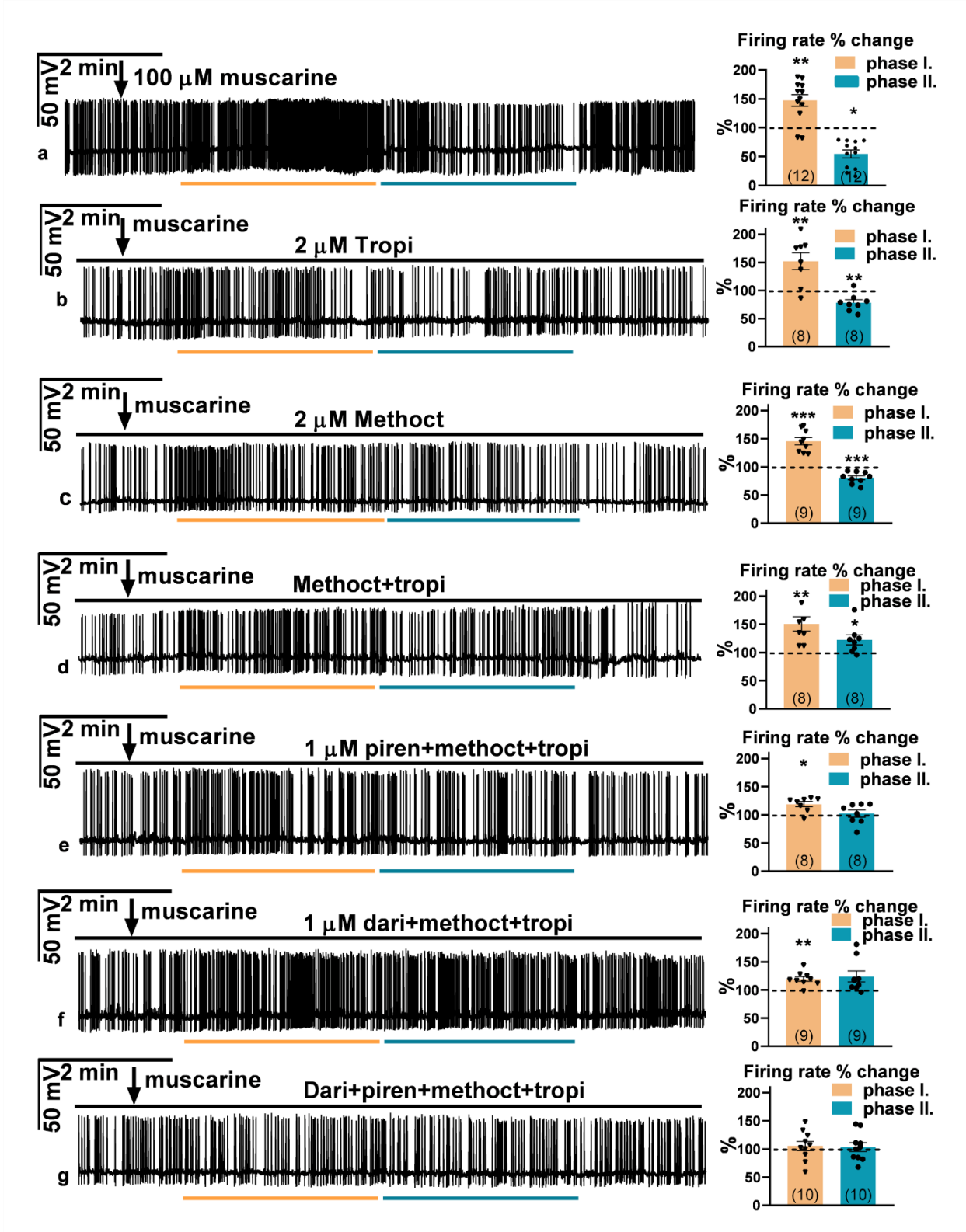

Fig 6. Impact of muscarine receptor subtypes on firing of GnRH neurons. Representative whole-cell patch current clamp recordings show that muscarine evoked a biphasic effect on firing of GnRH neurons expressing various muscarine receptor subtypes. **a**. In the first, ~2.5-minute period, muscarine (100 μM) enhanced (phase I) the firing rate of GnRH neuron followed by a decreased activity period (phase II). **b.** The inhibitory, M4-muscarine receptor antagonist tropicamide (2 μM) dampened the inhibitory effect of muscarine (as seen in phase II). **c.** The

inhibitory M2-muscarine receptor antagonist, methoctramine (2 μM) also decreased the inhibitory effect of muscarine (phase II). **d**. Co-administration of tropicamide and methoctramine eliminated the inhibitory effect of muscarine (phase II). **e**. The stimulatory, M1-muscarine receptor antagonist, pirenzepine (1 μM) dampened the stimulatory effect of muscarine (as seen in phase I) in the presence of the M2 and M4 antagonists. **f.** The stimulatory, M3-muscarine receptor antagonist, darifenacin (1 μM) also attenuated the stimulatory effect of muscarine (phase I). **g**. Neither facilitation nor inhibition was seen when a cocktail of all four antagonists was applied. Black line above each recording shows presence of cocktails of various muscarine receptor subtype inhibitors in the aCSF (dari=darifenacin, methoct=methoctramine, piren=pirenzepine, tropi=tropicamide). Light brown line under each recording presents period of stimulatory phase (phase I) and blue line stands for that of the inhibitory phase (phase II). Arrows show administration of muscarine. *=p<0.05, **<0.01, ***=p<0.005.

Optogenetic activation of cholinergic afferents changes the electrophysiological activity of GnRH neurons and reveals co-transmission of ACh and GABA

To study the effect of endogenous ACh, GnRH neurons of triple-transgenic, Chat-Cre-ChR2-GnRH-GFP mice were examined in acute brain slices using LED square pulses (470 nm, 5 ms) to activate channelrhodopsin-expressing cholinergic axons. GnRH neurons were whole-cell clamped in current-clamp mode at 0 pA to detect firing. After a 30 s control period LED train of 5 Hz was applied for a subsequent 60 s while firing was continuously recorded. Biphasic pattern was detected when 5 Hz train was applied: the initial stimulation (191.2 ± 33.19%, p=0.0157, t=2.748, df=14, t-test) was followed by a transient inhibition (71.0 ± 9.02%, p=0.0063, t=3.212, df=14). Stimulation lasted for 15 ± 2.7 s; inhibition lasted for 38 ± 3.4 s (**Fig 7a and 7c.**). Both stimulation and inhibition disappeared in the presence of a cocktail of atropine and mecamylamine (**Fig 7b and 7c.**), suggesting involvement of ACh in the process.

Effects of optogenetic activation of cholinergic afferents were seen in the membrane currents, too. After a 2 min control period, LED illumination of 5 Hz (2 min) induced an initial inward current (amplitude: 51 ± 12.7 pA, **Fig 7d and 7f.**) resembling those ones triggered by carbachol. A transient decrease in the frequency was then observed (80.2 ± 8.65 % of the control value, n=27 **Fig 7d and 7f**). Both inward current

and the decreased frequency were eliminated in the presence of atropine+mecamylamine (frequency: 118.9 ± 16.16 % of the control, n=8, **Fig 7e and 7f**). The difference in the frequency data was significant (Student's t-test, p=0.0405, df=33, t=2.132).

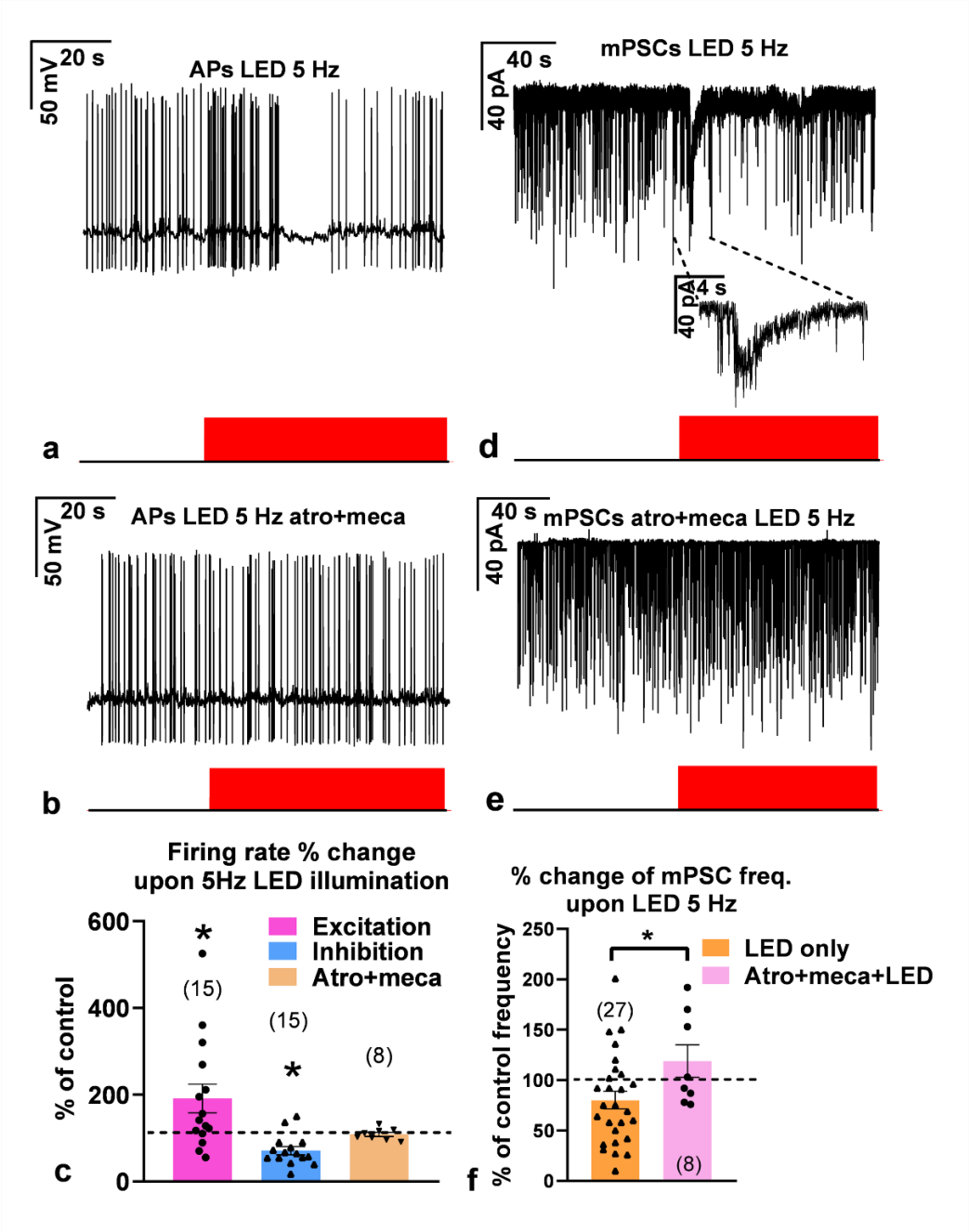

Fig 7. Effects of optogenetic stimulation of cholinergic axons upon firing activity and frequency of spontaneous mPSCs of GnRH neurons. **a**. LED illumination at 5 Hz evoked an initial facilitation followed by transient inhibition in firing. **b**. Both the stimulatory and inhibitory effects were eliminated when the slices were pretreated with the cocktail of atropine+mecamylamine. **c**. The bar graph summarizes the effect of LED illumination at 5 Hz revealing that ACh was released from channelrhodopsin enriched cholinergic terminals. **d.** LED of

5 Hz triggered an inward current followed by a transient decrease in the mPSC frequency. The inset is a zoomed region of the graph containing the inward current. **e.** Both the inward current and the diminished mPSC frequency disappeared in the presence of cocktail of atropine+mecamylamine. **f.** The bar graph shows a significant difference in the mPSC frequencies measured in the absence/presence of the inhibitor cocktail. Atro=atropine, meca=mecamylamine. Recordings are in black color, red bars underneath the recordings indicate the period of LED illumination. The numbers of the measured neurons are in parentheses. *=p<0.05.

To examine the extra- and/or synaptic character of cholinergic neurotransmission onto GnRH neurons, the existence/absence of evoked mPSC (emPSC) was investigated in the presence of TTX in GnRH neurons of the adult, male, Chat-Cre-ChR2-GnRH-GFP transgenic mice. LED illumination (0.2 Hz, 470 nm, 5 ms duration, then averaged of 60 runs of the 5 s long recordings) triggered no visible emPSC response in 90 % of GnRH neurons suggesting an extra-synaptic action of ACh. In 10 % of the cells, however, robust emPSC was seen (**Fig 8a**). The emPSCs occurred synchronously with the LED square pulse (**Fig 8, zoomed inset**). The onset was 2-3 ms after the rise of the illumination. The emPSC was still observable in the same GnRH neuron in the presence of atropine+mecamylamine (10-10 μM, **Fig 8b**) showing the release of a neurotransmitter/neuromodulator other than ACh.

In other GnRH neurons of triple transgenic mouse in which emPSC was evoked by LED of 0.2 Hz (**Fig 8c**), we examined the effect of a 5 Hz LED illumination (5 Hz train, then averaged of 60 runs of the 5 s long recordings). In 50 % of these neurons, train of emPSCs was seen (**Fig 8d**). These emPSCs were synchronous with the 5 Hz LED pulses, although, the amplitude was lower than the one evoked by the 0.2 Hz (≈20 %). To identify the transmitter(s) responsible for the emPSCs, first picrotoxin (100 μM) was added to the aCSF and existence/absence of synaptic response was examined at 0.2 or 5 Hz in the same GnRH neuron as in **Fig 8c and 8d**. Picrotoxin abolished the emPSC at 0.2 Hz completely, providing strong evidence for the exclusive release of GABA from ChR-2-tagged cholinergic axons (**Fig 8e**) at this LED frequency. Surprisingly, train of emPSCs was still detected at 5 Hz illumination (**Fig 8f**) in the presence of picrotoxin in this same neuron. Amplitudes of these emPSCs were lower than those detected without the GABA-A-R blocker. The emPSCs triggered by LED of 5 Hz were eliminated when atropine-mecamylamine was then

added to the aCSF beside picrotoxin (**Fig 8g**). The last two observations suggest the release of both ACh and GABA at 5 Hz frequency. These results show that cholinergic axons innervating GnRH neurons use ACh and GABA for neurotransmission in a frequency dependent manner.

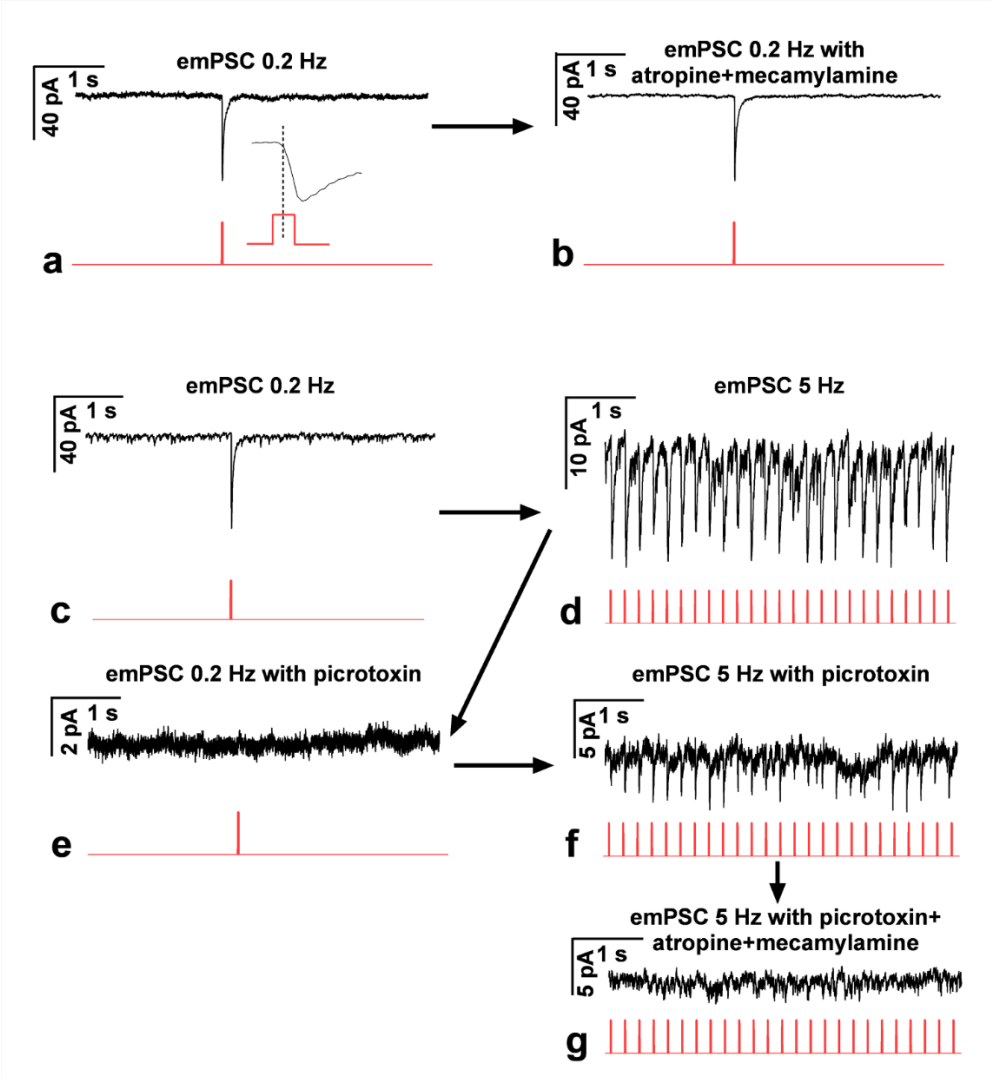

Fig 8. Evoked mPSCs (emPSCs) observed in a subpopulation of GnRH neurons of Chat-Cre-ChR2-GnRH-GFP transgenic mice upon LED illumination at 0.2 or 5 Hz. a. Robust inward emPSC was triggered by LED illumination at 0.2 Hz. **b**. The emPSC was still seen in the presence of atropine+mecamylamine in the same neuron as in **a**. **c**. Similar emPSC was revealed in another GnRH neuron at 0.2 Hz. **d.** Train of emPSCs of lower amplitude was evoked by LED at 5 Hz in the same neuron as in **c**. **e.** The emPSC observed at 0.2 Hz was eliminated by picrotoxin in the same neuron as in **d**. **f.** A train of emPSCs was still detected in the presence of picrotoxin at 5 Hz in the same neuron as in **e**. **g**. This train was abolished by adding atropine+mecamylamine to the picrotoxin-containing-aCSF in the same neuron as in **f**. Arrows show the time-order of

measurements in the same neuron. Recordings are in black color, red lines underneath the recordings indicate the period of LED illumination at 0.2 or 5 Hz, respectively.

The above optogenetic studies showed that GABA and acetylcholine are co-transmitted from a subpopulation of cholinergic axon terminals depending on the frequency of LED stimulation. To provide the structural correlate of ACh/GABA co-transmission, immunofluorescence triple labeling was performed on preoptic sections of Chat-Cre-ChR2 transgenic mouse brain for vesicular GABA transporter (VGAT), green fluorescent protein (GFP)-tagged channelrhodopsin-2 (ChR2-GFP) and GnRH. The confocal microscopic analysis revealed that VGAT-IR (**Fig 9a and 9b**), and cholinergic, ChR2-GFP-IR (**Fig 9a and 9c**) axons exist in the proximity of GnRH neurons. At high power, the VGAT (**Fig 9b**) and ChR2-GFP (**Fig 9c**) were co-localized **(Fig 9d)** in the same cholinergic axon varicosities. Furthermore, VGAT- (**Fig 9f**) and ChR2-GFP- (**Fig 9g**) expressing double-labeled axon boutons (**Fig 9e and 9i**) were found in juxtaposition (**Fig 9e and 9i**) with GnRH dendrite (**Fig 9h and 9i**). These morphological results unveiled the dual ACh/GABA chemotype of at least a subset of cholinergic axons innervating GnRH neurons and support the optogenetic findings on ACh/ GABA co-transmission in regulation of GnRH neurons.

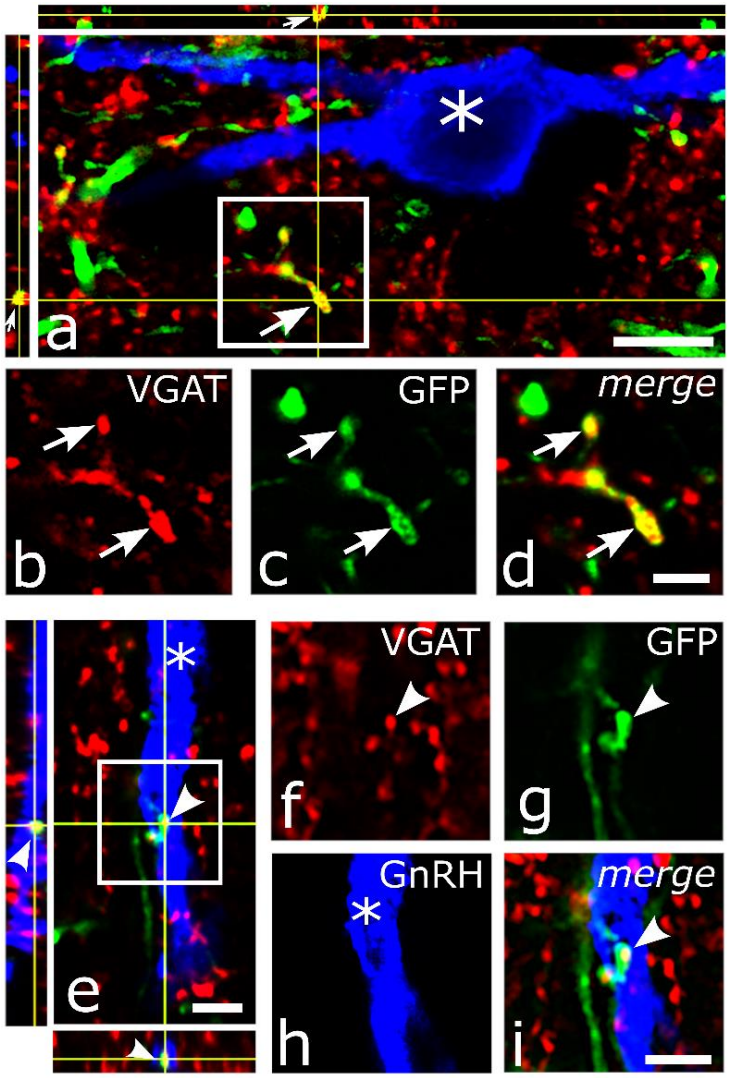

Fig 9. **Expression of vesicular GABA transporter in cholinergic axons targeting GnRH neurons in the Chat-Cre-ChR2 mouse.** (**a**) Triple immunofluorescent imaging revealed vesicular GABA transporter (VGAT, red channel), GFP- tagged channelrhodopsin-2 (ChR2-GFP, green) and GnRH (blue)-immunoreactive (IR) structures via confocal microscopy. VGAT (**b**) and ChR2-GFP (**c**) were co-localized (**d**) within the same axon varicosity (enframed in **a**, enlarged in **d**, arrows) near a GnRH neuron (blue, asterisk). The juxtaposition of a VGAT (**f**, arrowhead) and ChR2-GFP (**g**) IR double-labelled axon varicosity (**i**) with the dendrite of a GnRH neuron (**h**, asterisk) was confirmed in orthogonal views (**e**; enframed area enlargement in **i**). Scale bars: a, 5 µm; b - i, 2 µm.

Networking of central cholinergic neurons with GnRH neurons

Hypophysiotrophic GnRH neurons receive cholinergic innervation

For structural evaluation and quantitative analysis of the putative interneuronal communication of the central cholinergic and GnRH systems, double immunofluorescence labeling combined with 3DISCO method was used on paramedian sagittal slices of GnRH-GFP transgenic mouse brain that contained the distribution sites of GnRH neurons in the medial septum, the vertical limb of the diagonal band of Broca, the region of the organum vasculosum laminae terminalis, the medial preoptic area and the anterior hypothalamic area (**Fig 10**).

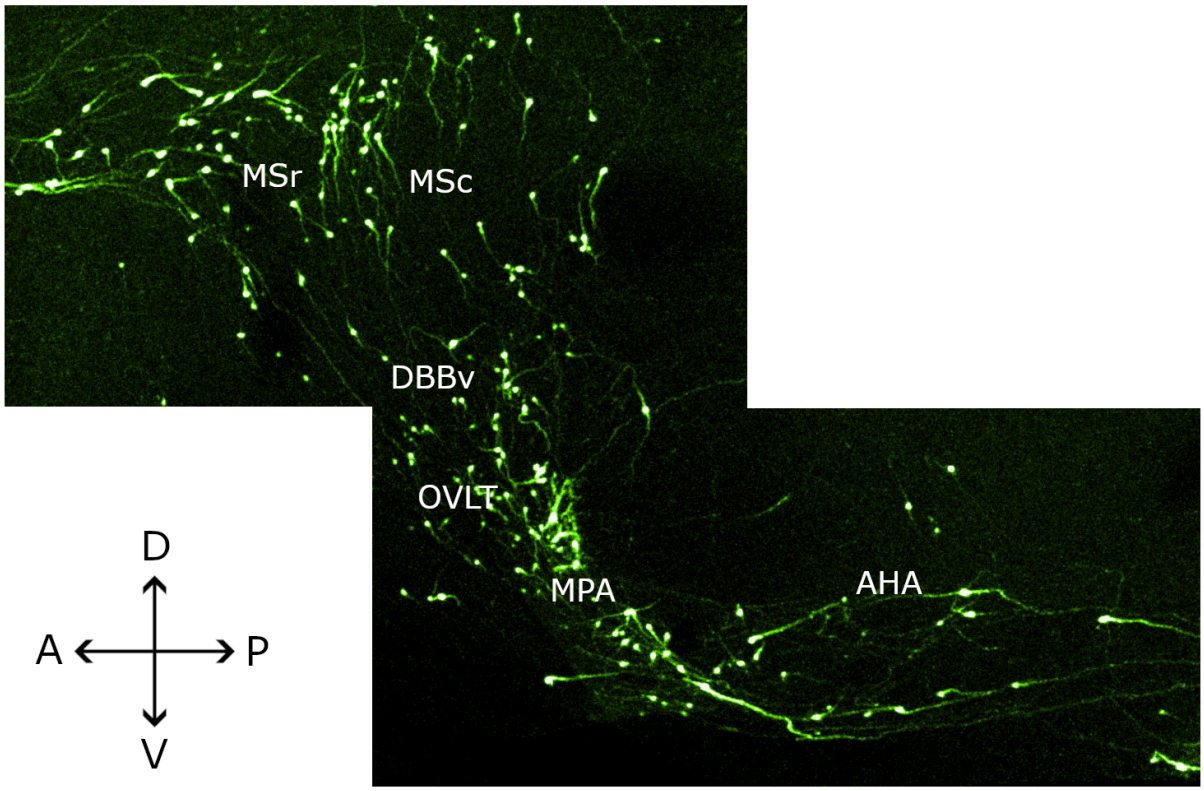

Fig 10. Distribution of GnRH-GFP-IR elements revealed by 3DISCO immunofluorescent microscopy. Thick brain slice (1 mm) cut in the paramedian sagittal plane. It represents the scanning areas used for image acquisition via confocal microscopy. MSr: medial septum, rostral part; MSc: medial septum, caudal part; DBBv: diagonal band of Broca, vertical part; OVLT organum vasculosum of the lamina terminalis; MPA: medial preoptic area and AHA: anterior hypothalamic area

The cholinergic axons were identified by their vesicular acetylcholine transporter (VAChT) content, whereas GnRH-immunoreactive (IR) profiles were visualized by immunostaining of the expressed green fluorescent protein (GFP). GnRH neurons were found to overlap with VAChT-IR axons **Fig 11a and 11b**) distributed in the sampled regions. Altogether, 4,899 optical slices (mean ± SEM: 816 ± 64 per brain) were evaluated. In each optical slice, the number of VAChT-IR axons juxtaposed to GnRH-IR perikarya, and dendrites were determined. Juxtapositions were justified with high precision in orthogonal view layout. Many VAChT-IR axon varicosities (1040 ± 96 SEM, n = 6) were identified in juxtaposition with GnRH-IR profiles (**Fig 11c and 11d**). Most of them (86.5 ± 3.2%) targeted GnRH dendrites (**Fig 11c**) and only a smaller fraction (13.5 ± 3.2 percent) contacted GnRH perikarya (909 ± 100.12 dendritic vs 131 ± 23.68 somatic input, n = 6; t-test, p = 1.928E-05; **Fig 11d**). In these samples, as an average, 37.4 ± 5.1 percent of reconstructed GnRH-IR perikarya (186 ± 20) received cholinergic inputs (68 ± 9.66 innervated vs 118 ± 16.9 non-innervated GnRH-IR perikarya, n = 6; t-test, p = 0.029).

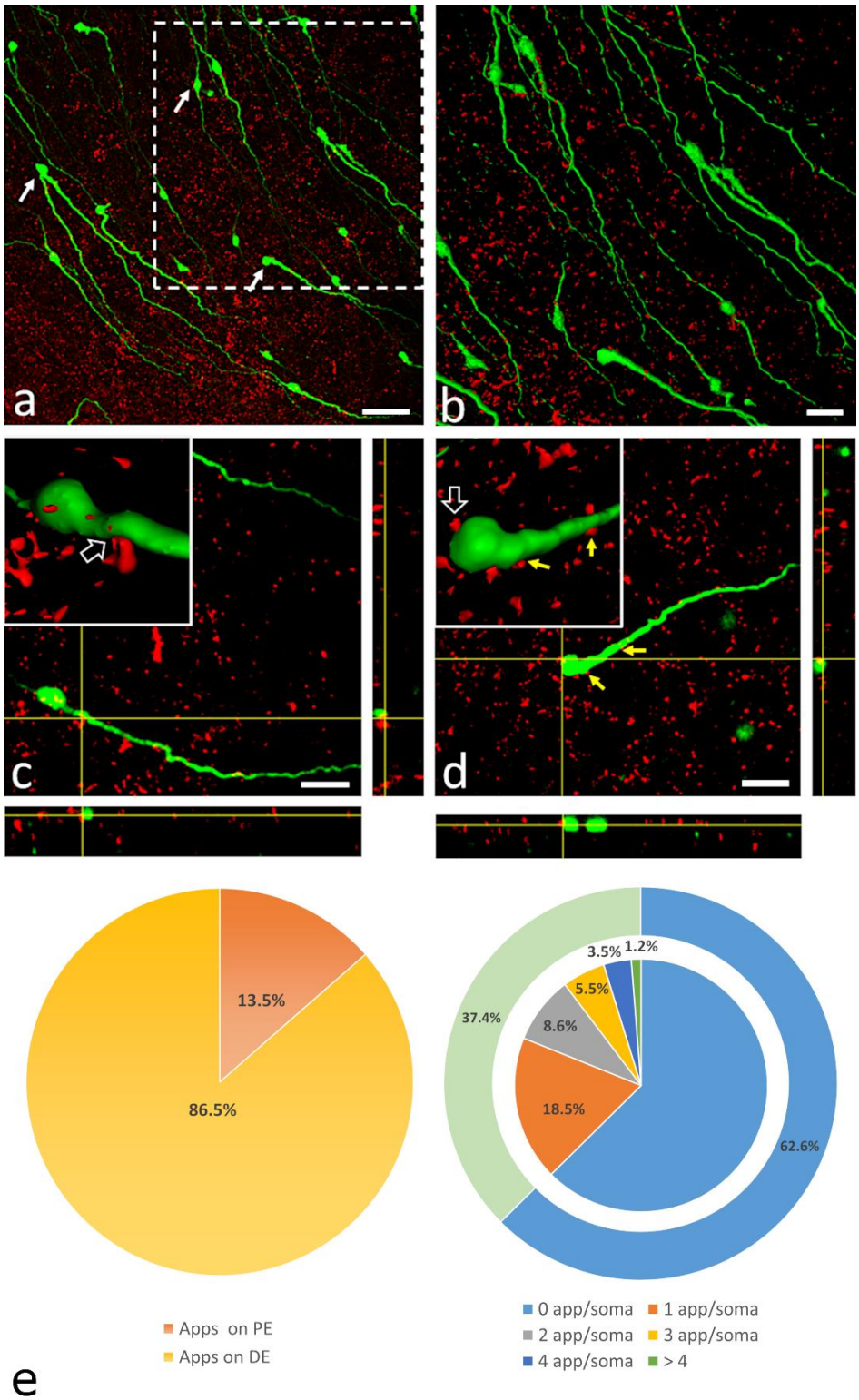

Fig 11. GnRH neurons receive cholinergic inputs as revealed by double immunostaining and 3DISCO method. a. A stack of confocal image planes projected in the z direction shows many GnRH neurons (green channel, arrows) and VAChT-immunoreactive (IR) axon varicosities (red channel). **b**. A part of the image stack shown by dashed square in **Fig 11a** was reconstructed as a 3D surface model using the ImageJ/Fiji software. Note the overlap of the two immunolabeled

systems. **c.** Axo-dendritic contact between a VAChT-IR axon and a GnRH neuron is shown in both 3D surface model (inset, arrow) and orthogonal views of stacks (yellow crosshairs). **d.** The inset shows an axo-somatic juxtaposition (empty arrow) in 3D image. The same communication site is confirmed in orthogonal views (yellow crosshairs). Two other cholinergic axon varicosities (yellow arrows) juxtaposed to the same GnRH neuron indicate the existence of multiple contact sites. **e.** The cholinergic axons communicate with GnRH dendrites (86.5%), the perikarya are less often targeted (13.5%). Apps on PE: appositions on perikarya, Apps on DE: appositions on dendrites. **f.** About one third (37,4 %) of the analyzed GnRH perikarya received VAChT-IR inputs. The inner pie diagram depicts the percentage distribution of VAChT-IR axon beads juxtaposed to the same GnRH perikaryon. App/soma: apposition per soma. Scale bars: a: 50 μm; b: 25 μm; c and d: 20 μm.

Ultrastructural correlates of networking

The networking among VAChT-IR axons and GnRH neurons was also confirmed at the ultrastructural level using pre-embedding double immunocytochemistry. For labeling of VAChT-IR axons nickel-3,3 diaminobenzidine (Ni-DAB) chromogen was used (**Fig 12a and 12b**), while the GnRH immunoreactive profiles were visualized by silver-intensified colloidal gold particles (**Fig 12c and 12d**). In the residence area of hypophysiotropic GnRH neurons, the medial septum-diagonal band of Broca-OVLT continuum, VAChT-expressing axons appeared in juxtaposition to cell bodies and dendrites (**Fig 12a**) and formed synapses (**Fig 12b)**. Based upon the different physico-chemical properties of the used chromogens, the GnRH and VAChT-IR profiles were clearly distinguishable from each other even at medium power electron microscopic screening (**Fig 12d**). The juxtaposition of cholinergic axon beads to dendritic and somatic domains of GnRH neurons without glial process interposition was confirmed at the ultrastructural level. Tracing the juxtaposed profiles through series of ultrathin sections occasionally revealed the synaptic engagement of VAChT-IR, cholinergic axons with dendrites (**Fig 12e**) and perikarya (**Fig 12f and 12g**) of GnRH neurons suggesting a direct regulatory influence of the cholinergic system upon the GnRH neuron assembly.

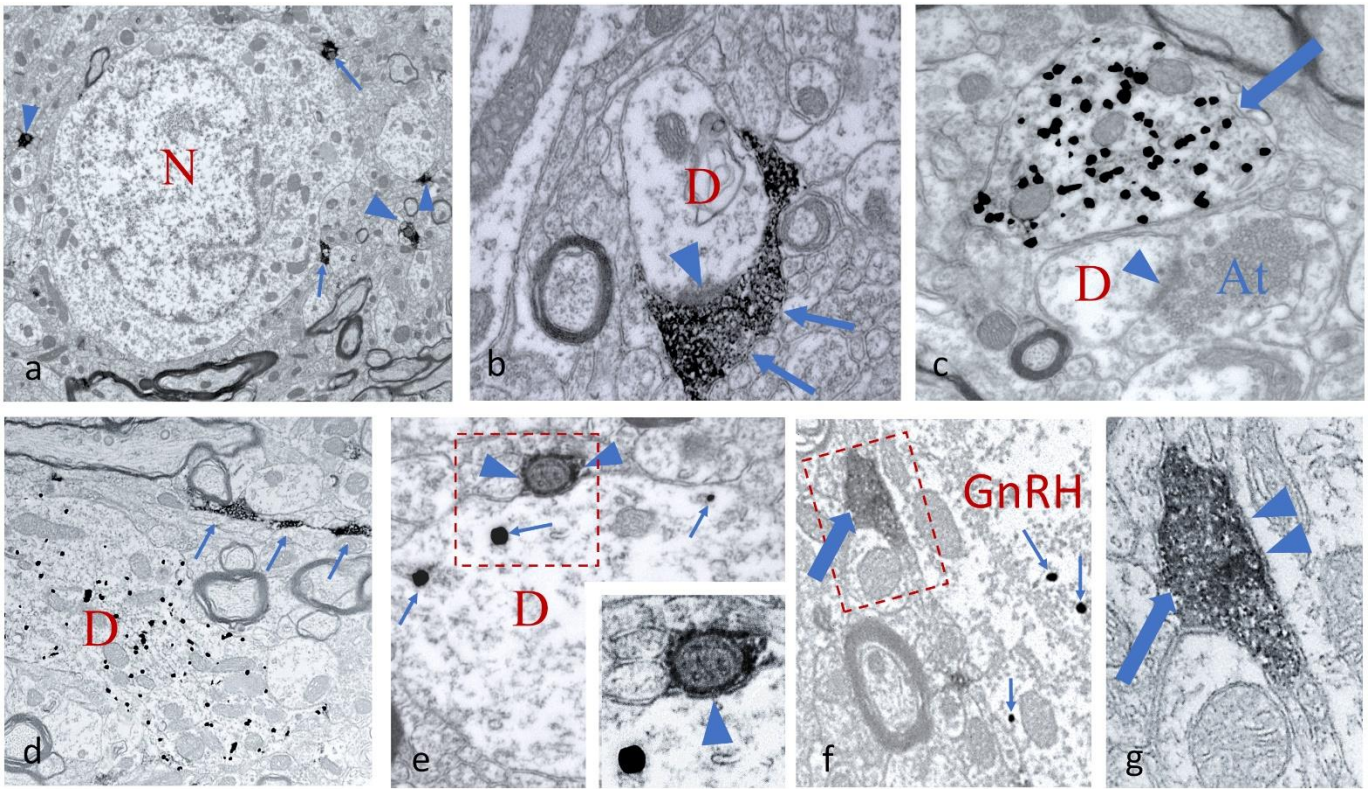

Fig 12. Ultrastructural detection of cholinergic axons and GnRH-immunoreactive (IR) profiles in the medial preoptic area (mPOA). a. Vesicular acetylcholine transporter (VAChT)-containing axons labeled by Ni-DAB chromogen are distributed in the neuropil of the mPOA contacting cell bodies (arrows) and dendrites (arrowheads). A non-labeled neuron (N) is in the center of micrograph. **b**. A Ni-DAB chromogen-labeled cholinergic axon (arrows) synapses (arrowhead) on a cross-sectioned dendrite (D). **c**. Appearance of a cross-sectioned GnRH dendrite (arrow) filled with silver-intensified, colloidal gold particles. A nearby unlabeled dendrite (D) receives a synapsing (arrowhead) axon terminal (At). **d**. Simultaneous detection of a longitudinally sectioned GnRH dendrite (D) identified by silver coated-colloidal gold particles and a varicose, longitudinally cut VAChT-IR axon (arrows) labeled by Ni-DAB chromogen. **e**. Cross-sectioned GnRH-IR dendrite (D) communicating with a small caliber cholinergic axon (arrowheads). Arrows point to the metallic label within the GnRH profile. The enframed region is shown at higher power in the inset, the arrowhead points to the postsynaptic membrane. **f.** Detail from a GnRH perikaryon (GnRH) that receives a cholinergic axon (thick arrow). Intensified, colloidal gold particles are labeled by small arrows. The communication site is enframed. **g**. High power view of the enframed area in **Fig f.** The labeled, cholinergic axon (thick arrow) filled with small-sized vesicles establishes synapse (arrowheads) with the GnRH perikaryon. Scale bars: **a**: 2 μm; **d**: 1 μm; **b** and **c**: 500 nm; **e-g**: 250 nm.

Identification of cholinergic neuronal source supplying innervation of GnRH neurons

To figure out which of the brain regions host cholinergic cells innervating GnRH neurons, a monosynaptic, rabies virus retrograde tract tracing technique was used [36, 37] in combination with immunocytochemistry. GnRH-Cre neurons (**Fig 13a and 13b**) expressing TVA receptor and G proteins became selectively infected by the modified, envelope protein A (EnvA)-coated, G-deleted rabies virus (RVdG). GnRH neurons expressed the TVA-GFP/TVA-receptor protein as the precursor neurons for rabies infection. (**Fig 13a**). No mCherry fluorescence of helper virus origin was seen in wild-type mice showing that the viral activation was Cre-dependent. Rabies virus-labeled neurons forming the primary afferents of the GnRH-Cre cells appeared in the entire length of the neuroaxis, with the highest number observed in the vicinity of the starter cells. Proceeding from the preoptic area toward the brain stem, their number gradually diminished. Detection of GFP fluorescence, indicator of rabies virus transfection, in choline acetyltransferase (Chat)-immunoreactive neurons identified the source of cholinergic afferents to GnRH neurons. These double-labelled neurons were in the medial septum (MS) and the diagonal band of Broca (DBB) (**Fig 13c and 13d**). No primary cholinergic afferent neurons were identified in other parts of the forebrain or in the brain stem indicating that the cholinergic regulatory input is local to the residence of GnRH neurons.

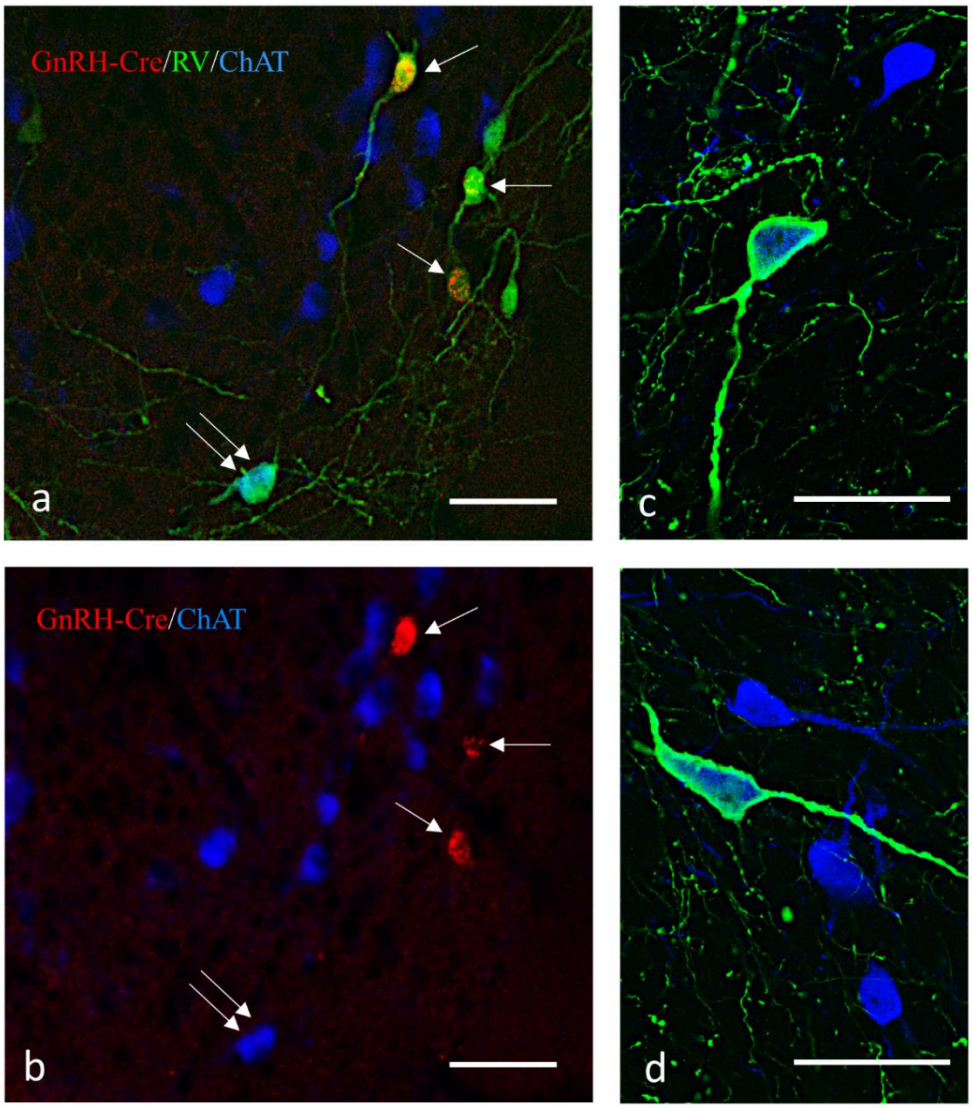

Fig 13. **Viral tracing of cholinergic afferents of GnRH neurons.** Monosynaptic tracing of primary afferents to GnRH-Cre neurons and subsequent immunohistochemical processing of brain sections identify AAVs-infected, Cre-positive neurons expressing mutated TVA and G protein fused to mCherry (in red), rabies virus-GFP infected cells (in green) and Chat-immunoreactive (IR) cells (in blue). Contrasting the mCherry signal, the green fluorescence fills both the perikarya and the processes. **a.** Starter cells (single arrows) express both mCherry and GFP, whereas the primary afferent neurons produce only GFP. Double arrows point to a cholinergic primary afferent neuron (in turquoise) having the mixture of both green and blue signals. **b.** Validation of double-labeled neurons by showing the fluorescent signals in single channels. **c and d**. Examples of Chat-IR cells labelled with the rabies GFP signal in the septo-diagonal band area of the mouse brain. Scale bar: 50 μm.

Pharmacogenetic activation of central cholinergic system *in vivo* increases secretion of luteinizing hormone (LH) in orchidectomized mice

To study the effect of an increased brain acetylcholine transmission upon secretion of luteinizing hormone (LH), a pharmacogenetic approach was used in transgenic *Chat-Cre-Gq DREADD* mice. Gonadal hormones are known to suppress the HPG axis via negative feedback, therefore, orchidectomized (ORX) animals were used that were accustomed to chronic handling prior to the experiment. The animal groups were composed of vehicle (DMSO) and clozapine-N-oxide (CNO)-administered mice. Blood samples were collected every 3 min over a 3 h period and their luteinizing hormone (LH) content was measured using an ultrasensitive ELISA technique [38]. We found that in the control group, DMSO administration had no influence upon LH secretion, the corresponding pre-treatment (basal LH: 4.92 ± 0.55 ng/ml; mean LH: 6.10 ± 0.66 ng/ml) and post-treatment (basal LH: 5.00 ± 0.59 ng/ml; mean LH: 6.17 ± 0.64 ng/ml) values didn't show significant differences (**Fig 14a-c**). In contrast, administration of CNO evoked a significant rise in both the basal (pre-treatment basal LH: 9.20±1.53 ng/ml vs post-treatment basal LH: 18.32 ± 2.21 ng/ml, paired t-test, p = 0.0104) and mean (pre-treatment mean LH: 11.21±1.74 ng/ml vs post-treatment mean LH: 23.07±3.50 ng/ml, paired t-test, p = 0.0266) LH values. (**Fig 14d-f**). The LH values peaked at 30 minutes after the initiation of CNO treatment. Characteristic, individual LH secretion patterns are shown in **S1 Fig**.

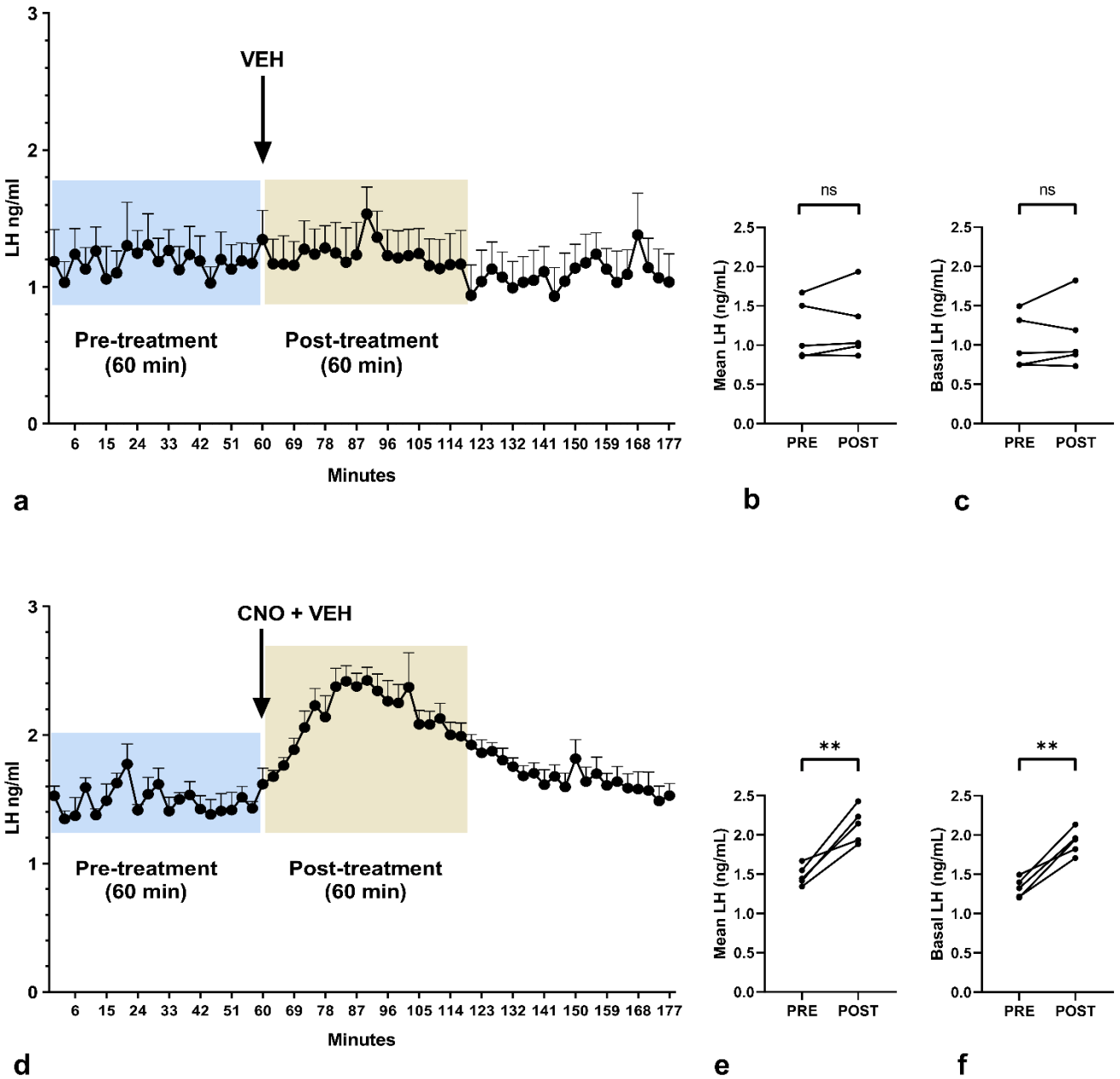

Fig 14. Effect of clozapine N-oxide (CNO) treatment on serum LH level in orchidectomized Chat-Cre-Gq DREADD mice. Blood samples were collected every 3 minutes over a 3-hour period. The LH concentration was determined using an ultrasensitive ELISA technique. The control (**a-c**) and CNO-treated (**d-f**) mice received vehicle or CNO, respectively, per os at the 60th minute from the onset of sampling. Graphs **a** and **d** show mean LH levels per sampling time revealed by ELISA. Comparing individual animals, the mean (**b**) and basal (**c**) LH serum levels remained unchanged within a 60 minute pre- and post-treatment period in the vehicle-treated control mice. In contrast, CNO treatment significantly increased both mean (**e**) and basal (**f**) serum LH concentration in the 60-minute post-treatment period (paired t-test; *$p < 0.05$).

Discussion

The study provides evidence for an important role of the central cholinergic system in the regulation of hypophysiotropic GnRH neurons and the reproductive axis. We found that 1.) ACh receptor agonists exert both facilitatory and inhibitory effects upon GnRH neurons. 2.) The released neurotransmitter, acetylcholine, binds to various functional nicotinic and muscarinic receptors expressed by GnRH cells. 3.) The cholinergic modulation is manifested in changes of both firing rate and frequency of mPSCs in GnRH neurons. 4.) Optogenetic stimulation of channelrhodopsin-2-expressing cholinergic axons modifies the electrophysiological activity of GnRH neurons and evokes GABA and ACh/GABA neurotransmission at 0.2 Hz and 5 Hz, respectively. 5). Cholinergic axons innervate and establish synaptic communication with GnRH neurons. 6.) The primary cholinergic afferents arise from medial septum and the diagonal band of Broca, regions where GnRH neurons are distributed 7). Pharmacogenetic activation of the central cholinergic system increases the secretion of luteinizing hormone (LH) in orchidectomized male mice. Collectively, the results suggest that acetylcholine tunes the operation of GnRH neurons via specific ACh receptors and the evoked *in vivo* biological response is activation of the HPG-axis.

Acetylcholine and carbachol modify the electrophysiological activity of GnRH neurons

We found that under whole cell current clamp measurements ACh (50 μM) evoked a biphasic effect upon the firing rate of GnRH neurons. First, a robust elevation was seen, followed by a gradual decline. Since electric activity of GnRH neurons and GnRH release (and concomitantly that of LH) correlate [39-41], the result suggests that during the first phase of ACh action GnRH neurons release a higher amount of GnRH, thereafter, the release becomes attenuated. To avoid the possibility that the decline in firing rate was due to inactivation of ACh by acetylcholinesterase, the measurement was repeated with carbachol (40 μM), a widely used AChR agonist not metabolized by the acetylcholine esterase. The biphasic action was observed again, the sequences and timing of the action was like those seen after ACh administration. In a recent report using embryonic GnRH neurons in nasal explant cultures [31], ACh was found to activate GnRH neurons by rapidly rising the intracellular Ca^{2+} concentration in the presence of GABA and glutamate receptor

blockers and the subsequent decline lasted for about five minutes. With regards to the involved mechanisms, the activation of α3 nAChR depolarized the cell membrane of embryonic GnRH neurons triggering further the opening of voltage-gated calcium channels (VGCCs) and calcium influx.

Thorough investigation of the recordings, however, shed light on that the first phase represented by elevated firing rate can be divided into two subphases. The first one is characterized by a relatively faster transient increase. After its decay, a slower and more prolonged rise in the firing rate was seen. The two subphases were found in both experiments carried out either with ACh or carbachol.

The faster, initial part of facilitation might represent the operation of ionotropic nAChRs. Our present qRT-PCR results also revealed the expression of different nAChRs in adult GnRH neurons. Therefore, we hypothesized the presence of functional nicotine ACh receptors. Indeed, pretreatment of the acute brain slices with mecamylamine, the broad-spectrum antagonist of nAChRs, eliminated the faster part, but leaving untouched the slow-type facilitation and the inhibitory phase. Hypothalamic expression of functional nAChRs has already been proven in POMC and NPY neurons of the arcuate nucleus and hypocretin cells in lateral hypothalamus where nicotine application enhanced their firing rate and depolarized their membrane [42]. Although the effect was indirect, firing of oxytocin neurons in the PVN was also modulated by nicotine [43]. Nicotinic regulation of GnRH release from fragments of medial basal hypothalamus was revealed, too [44]. Very recently, stimulation of embryonic GnRH neurons by nicotine has also been shown [31].

In our study we found that the slow facilitation and the inhibition of the firing did not change in the presence of mecamylamine suggesting that these slow components were due to the activation of metabotropic muscarinic AChRs. Indeed, application of the broad spectrum mAChR antagonist atropine abolished both slow components while the faster transient facilitation remained intact indicating expression of functional muscarinic receptors in GnRH neurons. Various hypothalamic neurons are under muscarinic modulation, such as CRF [45] and POMC cells [46]. Goldfish [47] and murine embryonic [31] GnRH neurons are also capable of responding to muscarine.

Our voltage clamp measurements presented here showed that carbachol triggered a strong inward current followed by a decrease in the frequency of mPSCs. Inward current indicates membrane depolarization suggesting that this phenomenon might cause the faster facilitation seen in firing upon carbachol application. The inward current was abolished by the broad-spectrum nAChR antagonist

mecamylamine indicating the inevitable role of nAChRs in the occurrence of the inward current. In the hypothalamus, similar nAChR-dependent activation was reported in POMC neurons [42]. Inward ion current and a correlated facilitation in the firing rate was also evoked by ACh in histaminergic tuberomammillary neurons of hypothalamic slices [48]. Embryonic mouse GnRH neurons also respond to ACh administration with a nAChR-dependent relatively faster and transient stimulatory change in membrane potential [49], resembling the appearance of carbachol induced inward current we observed in this study. The carbachol-triggered decrease in the frequency of mPSCs developing after the completion of the inward current was blocked by atropine showing the involvement of mAChRs in the process. Muscarinic modulation of GABAergic mIPSCs has been observed in rat histaminergic tuberomammillary neurons [50]. Earlier reports have also shown mAChR-dependent ion currents in goldfish [47] and mouse embryonic [31] GnRH neurons.

GnRH neurons express various functional nicotinic and muscarinic ACh receptors

Processing of the incoming modulatory signal of acetylcholine requires the possession of functional cholinergic receptors by GnRH neurons. Using quantitative real-time PCR study, we have shown the relative expression of all five muscarinic receptor genes (*m1-m5*) in pooled cytoplasmic samples of GnRH-GFP neurons. Earlier studies have found only expression of *Chrm1* [28] and *Chrm4* genes [51] in GnRH cells. In immortalized GnRH neurons (GT1-7 cells), mRNA transcripts for Ch*m1*, Ch*m2* and *m4* were identified [29, 30]. With regards to expression of nicotinic receptors, three alpha subunits (*Chrna*3, *Chrna4 and Chrna7*) and three beta subunits (*Chrnb2*, *Chrnb3 and Chrnb4*) appeared in our samples. Earlier studies have confirmed the expression of *Chrb1, Chrb2, Chrnb4 and Chrng* genes in mouse GnRH neurons [28, 52, 53]. GnRH neurons - at an early stage of development - in explant culture of the nasal placode - process the ACh signal via alpha 3 nicotinic and M2 and M4 muscarinic receptors [31]. The differences seen in signaling mechanisms of ACh in embryonic *versus* mature GnRH neurons suggest that differentiation and integration of the cells at the destination sites of their migration with cholinergic neurons reshape the profile of the used, functional ACh receptors. Collectively these data indicate that both ionotropic and metabotropic receptors relay ACh-mediated information to GnRH neurons in mice.

Nicotine triggered a robust inward ion current in GnRH neurons, indicating a stimulatory effect when nicotinic receptors were activated. Similar nicotine-evoked activation of POMC and NPY neurons were reported in the arcuate nucleus [42]. The responses evoked by repeated application (90-120 s) of nicotine presented no desensitization which fits the observation that desensitization of nAChRs can disappear in less than 1 min [42, 54].

Regarding the nicotine receptor-mediated modulation, our ion current measurements dissected the subunit compositions of the involved nAChRs. Using various specific antagonists and agonists, the presence of α3β4, α4β2 and α7 receptors was revealed in GnRH neurons. The measurements using α3β4 and α4β2 antagonists applied to the same neuron in different sequence also showed that a GnRH neuron expressing α4β2 also expresses α3β4 and *vice versa*. The hypothalamic presence of functional α4β2 and α7 receptors has previously been demonstrated [42], and expression of α3 subunit was recently revealed in embryonic GnRH neurons [31]. It is worthy of note that α4, α7, β2 and β4 receptors were not found in these embryonic neurons [31], indicating potential differences in cholinergic receptor sets displayed by adult *versus* embryonic GnRH neurons. Analyzing the amplitudes of the inward ion currents evoked by activation of the nAChRs composed various subunits suggested that the most abundant versions are the ones of α4β2 and α3β4 while involvement of α7 seems minor compared with the two others, although significant contribution of this subtype to the nicotinic activation in other hypothalamic areas was reported [31, 55].

The patch clamp measurements presented here supplied unambiguous evidence for the expression of functional M1-M2-M3-M4 subtypes of mAChRs in GnRH neurons. Muscarine administration first increased, thereafter, decreased the firing rate of GnRH cells. Pretreatment with various subtype specific antagonists of mAChRs demonstrated that the facilitation was due to the activation of M1 and M3 subtypes, whereas M2 and M4 receptors were responsible for the decreased firing rate. The M1 and M3 receptors are coupled to G_q proteins known to execute stimulation, in contrast to the M2 and M4 receptors coupled to $G_{i/o}$ proteins triggering inhibition [56]. Presence of the inhibitory M2 and M4 receptors was also confirmed in embryonic GnRH neurons whose activation triggers the dissociation of the G-protein and its βγ subunit activates the G-protein-gated inwardly rectifying potassium (GIRK) channel that drives a hyperpolarization in the membrane potential [31]. The involvement of the stimulatory M1 and M3 receptors in the regulation of embryonic GnRH neurons has not been stated. It seems that not only the nicotinic but also the muscarinic

regulation is different in adult *versus* embryonic GnRH neurons. It is worthy of note that in the presence of M2 or M4 antagonists the stimulatory phase lasts longer than in the absence of these inhibitors indicating that one of the functions of M2 and M4 receptors in GnRH neurons is to compensate facilitation and restore the basic condition of the neuron [31].

Examination of the effect of muscarine on the mPSCs demonstrated that muscarine increased the frequency of the mPSCs when M2 and M4 receptors were blocked by a cocktail having tropicamide and methoctramine. In contrast, frequency decreased upon muscarine application in the presence of the M1 and M3 antagonists, darifenacin and pirenzepine, respectively. Both facilitatory and inhibitory actions were abolished by the intracellular application of tetrahydrolipstatin (THL) blocking the endocannabinoid 2-AG synthesis. The tonic release of 2-AG in GnRH neurons is behind this phenomenon, explaining how level of this endocannabinoid can be increased/decreased resulting in inhibition/facilitation of the excitatory GABAergic input by a retrograde signalling mechanism [10, 57]. Involvement of the endocannabinoid retrograde signalling in the regulation of GnRH neurons has already been reported under various physiological challenges [10, 12, 57, 58]. The role of endocannabinoids in the mediation of the effects of activated mAChRs has also been described in various brain regions including the thalamus [59], the striatum [60] and the cerebral cortex [61-63]. In addition, our present measurements with the intracellularly applied THL suggest that m1-m4 receptors are postsynaptic in GnRH neurons.

The above discussed results substantiated that GnRH neurons receive acetylcholine signals that exert a direct neuromodulatory influence via both muscarinic and nicotinic receptors displayed by GnRH cells.

Cholinergic innervation of hypophysiotropic GnRH neurons

In mice, GnRH neurons form a loose neuronal network in the medial septum (MS), the diagonal band of Broca (DBB) and the medial preoptic area (mPOA) [64] continuum. This anatomical formation is surrounded by clusters of acetylcholine-synthesizing neurons in the MS and DBB [65, 66]. Due to this unique allocation, both cholinergic and GnRH neurons often appear intermingled at the same anatomical site. The MS-DBB-mPOA region is also rich in VAChT-immunoreactive axons [67] indicating that ACh might exert control upon several neuronal phenotypes in this area. The accomplished quantitative structural

analysis has revealed that hypophysiotropic GnRH neurons are innervation targets of scattering cholinergic axons. The applied 3DISCO immunocytochemical technique allowed us to study the putative interaction of cholinergic axons with perikarya and dendrites of GnRH neurons distributed in thick forebrain slices. The confocal laser microscopic evaluation of the double-labeled specimens confirmed the juxtaposition of VAChT-IR axons to somatic and dendritic domains [68] of GnRH neurons. Each detected juxtaposition was confirmed in orthogonal views of optical slices. Most of the analyzed cholinergic axons were juxtaposed to dendrites (86.5 ± 3.2 percent) of GnRH neurons and a much smaller fraction appeared to innervate the somata (13.5 ± 3.2 percent) of the hypophysiotropic cells. The exquisite role of GnRH dendrites in communication with other classic neurotransmitter systems has previously been reported [69]. It is of note, that, as an average, 37.4 ± 5.1 percent of reconstructed GnRH-IR perikarya received cholinergic inputs indicating a preferential cholinergic neuronal control also at the level of cell bodies. Both single and multiple types of cholinergic communication sites were found on the surface of reconstructed GnRH cell bodies. In a recent paper, a rich cholinergic innervation of mouse GnRH perikarya was reported in female and male mice with high abundance of interacting profiles in the medial septum and DBB [31]. The observed axo-dendritic and axo-somatic juxtapositions observed in our study were analyzed further with high resolution, double immunoelectron microscopic technique. The applied, distinct electron-dense markers (silver-intensified colloidal gold and nickel intensified 3,3-diaminobenzidine) clearly identified GnRH-producing neurons and VAChT-IR axons. The cholinergic axons formed synaptic connections with neurons in the MS-DBB-mPOA region. Such terminals were filled with small sized, electron lucent vesicles from which the released transmitter can reach its receptors and initiate wired, synaptic- and/or volume transmission-type actions [70]. The ultrastructural analysis has confirmed the findings of the 3DISCO immunocytochemical study showing that the juxtaposed VAChT- and GnRH-IR neuronal profiles directly contacted each other without interposing astrocytic processes and the cholinergic axons established synapses with GnRH neurons. Similar synaptic networking between cholinergic axons and GnRH neurons has previously been reported in the rat [71].

Cholinergic neurons residing in medial septum and diagonal band of Broca supply the hypophysiotropic GnRH neurons

Cholinergic cell groups show an extensive distribution in the mouse brain [65] and many of the host regions project to the medial septum-diagonal band of Broca-medial preoptic area where GnRH neurons reside. To find cholinergic neurons that are synaptically linked to GnRH cells, a monosynaptic, rabies virus retrograde tract tracing from mouse GnRH-Cre neurons was used in combination with immunodetection of the cholinergic marker enzyme, choline acetyltransferase. The used GnRH-Cre transgenic mouse line has previously been characterized by high percentage of GnRH neurons (96%) expressing Cre recombinase [72]. Studying all cholinergic cell groups and clusters of the brain revealed that rabies virus-labeled, ACh-synthesizing neurons appeared exclusively in the medial septum and the diagonal band of Broca. Targeting the GnRH-Cre cells with rabies virus resulted in retrogradely labelled neurons in diverse brain regions like those published previously using different transsynaptic, retrograde tract-tracing techniques [7, 72].

The finding suggests that the primary, cholinergic afferents of GnRH neurons arise from a local source. The medial septum has also been claimed as the main source of cholinergic neuronal inputs to embryonic GnRH neurons by showing the Chat-IR fibers communicating with GnRH neurons also have p75 nerve growth factor receptor (p75NGFR), the specific marker of basal forebrain cholinergic neurons [31]. It is of particular interest that most septo-hippocampal cholinergic neurons synthesize and co-transmit GABA [73]. GABA exerts a powerful, excitatory effect upon hypophysiotropic GnRH neurons via GABA-A receptor [17, 57, 74], although, the anatomical sites of its production [75-77] have not been fully explored yet. Therefore, we examined further the nature of cholinergic inputs to elucidate whether GABA is released from the currently identified cholinergic afferents of GnRH neurons.

Optogenetic activation of cholinergic axons changes firing rate and the frequency of mPSCs of GnRH neurons and evokes a frequency dependent co-transmission of ACh and GABA

LED illumination of GnRH neurons at 5 Hz in Chat-Cre-ChR2-GnRH-GFP transgenic mice evoked a biphasic change in the firing rate like that observed upon ACh or carbachol administration suggesting that this modulation was due to endogenous ACh release from axons innervating GnRH neurons. The stimulation

followed by inhibition resemble recent results from embryonic GnRH neurons [31]. The LED-evoked changes in firing rate were abolished by combined administration of mecamylamine and atropine. The LED illumination also induced changes in the membrane current. First, it evoked an inward current, then it decreased the frequency of mPSCs. Antagonization of nicotinic and muscarinic ACh receptors prevented both effects. The observations are in line with our current pharmacological results showing that nicotinic AChRs are involved in the development of the inward current and muscarinic receptors are responsible for the modulated frequency of mPSCs.

LED illumination at 0.2 or 5 Hz resulted in a frequency dependent evoked response. Our measurements revealed that exclusive GABA release was evoked from cholinergic axons at LED illumination at 0.2 Hz. In contrast, both GABA and ACh were released from axons innervating GnRH neurons at LED illumination of 5 Hz. Co-transmission of ACh and GABA has already been demonstrated in hippocampal neurons [73], however, their accidental frequency dependency has not been investigated, yet. Similar co-transmission of neuropeptide and GABA was shown from AVPV kisspeptin neurons contacting GnRH neurons [77]. Nevertheless, a frequency-dependent release mechanism has also been revealed in hypothalamic kisspeptin neurons of mice [78, 79] where low frequency optogenetic illumination liberated GABA from the peptidergic axons and the high frequency challenge evoked kisspeptin release. In addition, our optogenetic results demonstrated that ACh exerts both synaptic and extrasynaptic effects on GnRH neurons.

Acute pharmacogenetic activation of central cholinergic neurons increases luteinizing hormone secretion

The results of the current *in vitro* electrophysiological studies show that ACh changes the frequency of both mPSCs as well as the firing rate in GnRH neurons. The former action is indicative of a direct targeting of GnRH neurons by cholinergic neurotransmission. The response seen in firing may imply indirect effects relayed by diverse primary afferent neuronal systems of GnRH cells that receive cholinergic modulation. The cholinergic neuron clusters – with dedicated regulatory missions within the CNS -are distributed throughout the neuroaxis [65], therefore, we used a pharmacogenetic approach to activate the central cholinergic system and study its effect upon GnRH-triggered luteinizing hormone (LH) secretion. In orchidectomized Chat-Gq (hM3Dq) DREADD transgenic mice treated with vehicle, the pre- and post-

treatment basal and mean serum LH levels were similar indicating that DMSO had no effect on LH secretion and the applied handling procedure successfully prevented the incidence of stress during the blood sampling via tail-cuts. Activation of hypophysiotropic corticotropin-releasing hormone (CRH) neurons in the hypothalamic paraventricular nucleus, the main regulators of the pituitary-adrenal axis and controllers of stress response, has recently been reported to inhibit pulsatile LH secretion [80] via acting on local GABAergic neurons [81]. In our study, activation of DREADD receptor-expressing cholinergic neurons by CNO administration increased both the basal and the mean LH values in a fast manner. LH level peaked at about 30 minutes after the CNO administration, then showed a prolonged return toward the basal level. These findings favor the view that acetylcholine activates the HPG axis. Similar conclusion has been drawn earlier by Martini's group showing that cholinergic drugs increase the secretion of LH under *in vitro* co-incubation of hypothalamus and anterior pituitary. The effect was potentiated by the acetylcholinesterase inhibitor, prostigmine and abolished by pretreatment with atropine [24]. Of note, acetylcholine did not increase the LH output when the medium contained exclusively anterior pituitaries indicating that the site of action was within the hypothalamus, presumably at the level of GnRH neurons. In concert with this report, injection of atropine into the third cerebral ventricle blocked the proestrus surge of LH and FSH in regularly cycling rats [82]. Cholinergic drugs also change the activity of GnRH neurons growing in cultured nasal explants where ACh and nicotine trigger the rise of calcium in GnRH cells followed by a long-lasting decline [49].

To sum up (**Fig 15**), in this study we showed that ACh is a powerful regulator of mouse GnRH neurons via the expressed nicotinic and muscarinic receptors. The direct cholinergic input originates from forebrain regions, the medial septum, and the diagonal band of Broca. The ACh-evoked effect is biphasic, consisting of an initial activation and a subsequent inhibition. Optogenetic stimulation of cholinergic axons results in a frequency-dependent co-transmission of ACh and GABA. The pharmacogenetic stimulation of the central cholinergic system *in vivo* evokes the activation of the HPG axis.

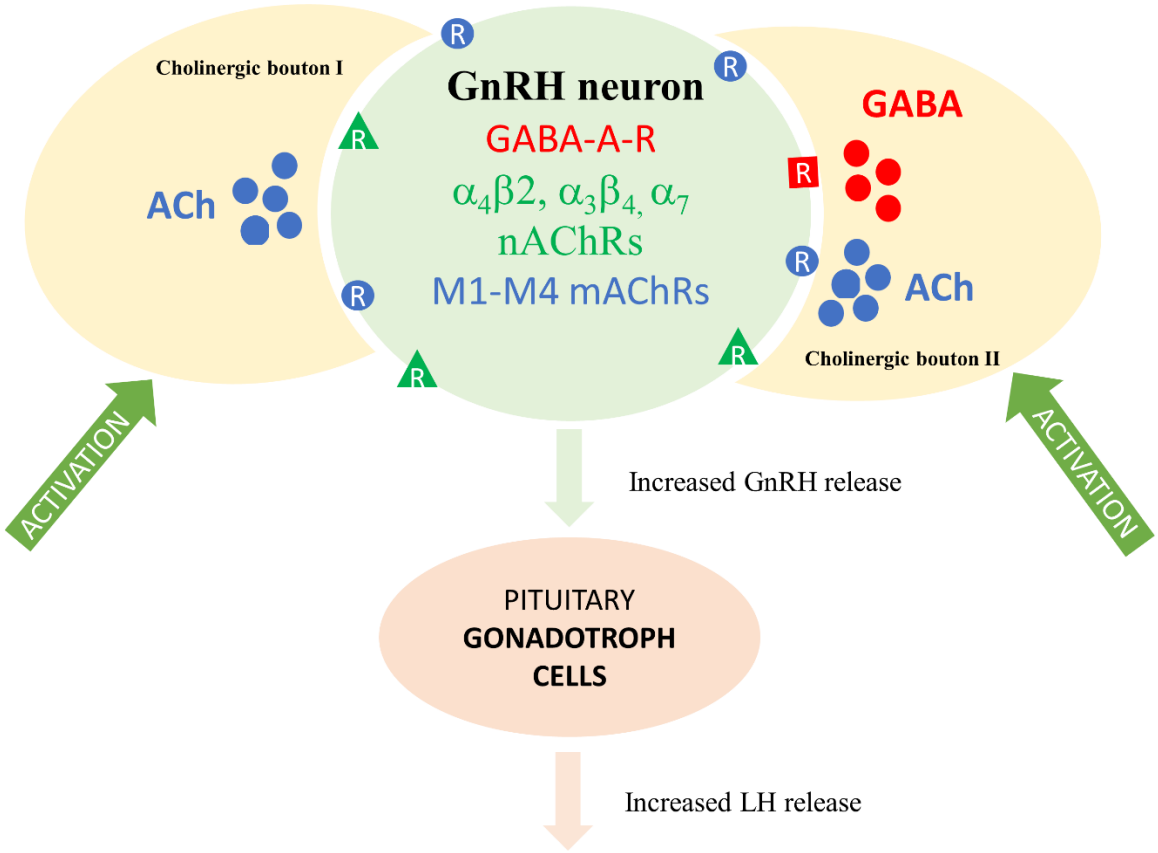

Fig 15. Schematic illustration of cholinergic control of GnRH neurons and HPG axis. Cholinergic boutons (I) innervate hypophysiotropic GnRH neurons that express GABA-A receptor (GABA-A-R, red square), three subtypes (α4β2, α3β4 and α7, green triangle) of nicotinic acetylcholine receptor (nAChR) and muscarinic receptors (M1-M4, mAChR, blue oval). The released ACh utilizes both muscarinic and nicotinic receptors in communication with GnRH neurons. At least a subpopulation of cholinergic boutons (II) is capable of transmitting gamma-aminobutyric acid (GABA) in addition to acetylcholine (ACh). Activation of cholinergic boutons increases the firing of GnRH neurons leading to increased GnRH and concurrent luteinizing hormone (LH) release.

Materials and Methods

Ethics

All experiments were performed in accordance with the Institutional Ethical Codex and the Hungarian Act of Animal Care and Experimentation guidelines (40/2013, II.14) which are in concert with the European Communities Council Directive of September 22, 2010 (2010/63/EU). The Animal Care and Experimentation Committee of the Institute of Experimental Medicine and the National Scientific Ethical Committee on Animal Experimentation have also approved the experiments under the project numbers PE/EA/796-5/2021, PE/EA/00646-2/2022.

Animals

Adult, male and female wild-type, and transgenic mice on the C57Bl/6 J or Bl6Fx background were used from local colonies bred at the Medical Gene Technology Unit of the Institute of Experimental Medicine (IEM). All animals were housed in a light (12:12 light–dark cycle, lights on at 06:00 h) and temperature (22 ± 2 °C) controlled environment, with free access to standard food and tap water. All surgical interventions and perfusions were carried out under deep anesthesia by intraperitoneal injections of a cocktail of ketamine (25 mg/kg body weight) and xylazine (5 mg/kg body weight).

Transgenic mouse lines and characterizations

The GnRH-GFP mouse line

The GnRH-GFP transgenic mouse line was generated to facilitate the study of hypothalamic GnRH neurons in which the green fluorescent protein (GFP) is genetically targeted to these cells [83]. The expression of GFP was detected in 84–94% of GnRH immune-positive neurons. This mouse line was used in studies aimed at electrophysiological characterization [10, 39, 57, 84, 85] and cell type-specific, genomic analysis of the GnRH neurons [28, 52, 53].

The Chat-Cre mouse line

Chat-IRES-Cre knock-in mice that express Cre recombinase in cholinergic neurons were bought from the Jackson Laboratory (JAX stock #006410). The line was rederived at the Medical Technology Unit of the IEM, Hungary [86]. Stock #006410 animals were bred to ROSA26::FLPe strain to facilitate the removal of the *frt*-neo cassette between the Cre and SV40 poly(A) to exclude ectopic Cre expression. The resulting

animals with the Chat-Cre-Δneo knock-in allele were bred together, while the ROSA26::FLPe was removed, to establish the chat/cre_Δneo//Gt(ROSA)26Sor/CAG/LSL mouse line.

The Chat-Cre-ChR2 mouse line

Chat-Cre-Δneo male mice were crossed with channelrhodopsin-2(ChR2) reporter mice [Ai32(RCL-ChR2(H134R)/EYFP), JAX stock #012569, for the purpose of optogenetics and morphological studies [87]. Offspring were genotyped for both Cre and enhanced yellow fluorescent protein (eYFP) transgenes to measure the copy number of the transgenes using YFP reference gene assay mix. Animals homozygous for Cre and eYFP were selected for morphological experiments, as well as for crossbreeding with the GnRH-GFP mouse line. The cholinergic neuron-specific expression of ChR2 was confirmed by double immunofluorescence staining for choline acetyltransferase (*Chat*) enzyme and (eYFP), (**S2 Fig**).

The Chat-Cre-ChR2-GnRH-GFP mouse line

The triple-transgenic, Chat-Cre-ChR2-GnRH-GFP mouse line was established for the purpose of optogenetic study using *in vitro* acute brain slice electrophysiology. In this experimental design, blue LED (470 nm) light stimulation of the ChR2-expressing axons of cholinergic neurons distributed in the medial preoptic area and whole cell patch recording from GFP-expressing GnRH neurons were performed simultaneously. To carry out this goal, homozygous male Chat-Cre-ChR2 mice were crossed with female GnRH-GFP mice. The presence of GnRH-GFP transgene in the offspring of the first generation was confirmed using real-time qPCR: the relative copy number of the gfp transgene (3 vs 2) was distinguishable using this method. The immunocytochemical phenotyping confirmed that GnRH neurons receive innervation from channelrhodopsin-2 expressing cholinergic neurons (**S3 Fig**).

The Chat-Gq (hM3Dq) DREADD mouse line

Chat/Cre_Δneo mice were crossed with B6N;129-Tg(CAG-CHRM3*,-mCitrine)1Ute/J mice (The Jackson Laboratories, JAX stock #026220) to express designer receptors (DREADD) signaling via Gq (hM3Dq) [88] in cholinergic neurons. This mouse line was used for chemogenetics. Its immunocytochemical characterization revealed mCitrine expression in Chat-immunoreactive neurons of the brain. The established new mouse line was used for *in vivo* chemogenetic activation of the cholinergic system including those subsets of cholinergic neurons that modulate the hypothalamic control mechanisms of reproduction. The

immunocytochemical phenotyping of the transgenic mouse strain confirmed the cholinergic neuron-specific expression of the excitatory hM3Dq DREADD receptor (**S4 Fig**).

The GnRH-Cre mouse line

Transgenic mice expressing Cre recombinase in GnRH neurons (GnRH-Cre) were used to determine brain regions that host cholinergic cells innervating GnRH neurons. The generation and characterization of this mouse line was published elsewhere [72]. Briefly, a 212 kb bacterial artificial chromosome (BAC) holding the entire *GnRH* coding sequence was modified: a *Cre recombinase-poly(A)* cassette was inserted into the ATG of the first exon of the *GnRH* gene, resulting in a high (over 96 percent) co-localization rate of the anti-Cre and anti-GnRH immunoreactivities [72].

Immunocytochemistry

Fluorescent immunocytochemistry

Adult, intact (n=15) and transgenic mice (n=20) were perfused transcardially with 4% paraformaldehyde (pH = 7.6, in PBS) for 10 min at a flow rate of 4 ml/min. Brains were removed rapidly from the skulls and post-fixed in the same fixative overnight at 4 C. On the next day, brains were sectioned in the coronal plane at 25 μm thickness using a Vibratome (Leica Inc, Wetzlar, Germany). Sections containing the medial septum (MS), diagonal band of Broca (DBB) and medial preoptic area (mPOA) were pre-treated with 0.5% H_2O_2 and permeabilized with 0.5% Triton X-100 for 20 min. The following primary antisera were used: anti-GnRH [raised in guinea pig #1018, diluted in 1:10.000 (gift from E. Hrabovszky)], anti-GFP (raised in either rabbit [Millipore #AB10145, 1:2.000 dilution]) and anti-VAChT (raised in rabbit, 1:5000 dilution) anti-vesicular GABA transporter (VGAT, raised in goat, 1:2500 dilution) and anti-Chat (Millipore #AB144P, raised in goat, 1:500 dilution). Secondary antisera (Alexa 488 conjugated anti-rabbit IgG; Cy3 conjugated anti-goat IgG, Cy5 conjugated anti-guineapig [Jackson ImmunoResearch Europe Ltd, UK]) were all diluted at 1:1000 in serum diluent (2% normal horse serum in PBS).

3DISCO technique

Adult, male GnRH-GFP transgenic mice (n=6) were perfused, and the brains were post-fixed as described in the previous section. Brains placed in a mouse brain mold were sliced at 1 mm thickness in the sagittal plane. Thereafter, double fluorescent immunocytochemistry combined with the 3DISCO technique [89]

were applied [90]. Briefly, the slices were rinsed several times in PBS, then were permeabilized with 0.5% Triton-X100 in PBS containing 0.1% gelatin and 0.05% merthiolate (PBS-GT) for 3 days at room temperature (RT) under constant agitation. For fluorescent immunocytochemical double labeling, brain slices were incubated with the anti-GFP (goat; #AB5450 Abcam, Cambridge, UK) and anti-VAChT (rabbit; generated by M. Watanabe, Hokkaido University, Japan) primary antibodies diluted in 1:5000 in PBS-GT for 7 days at RT. Several washes (6 x 60 mins) in PBS-GT were followed by the incubation with secondary antibodies (1:500; Cy3 anti-goat IgG and Cy5 anti-rabbit IgG; Jackson ImmunoResearch Europe Ltd., Cambridge House, UK) for 7 days at RT.

Slices were then rinsed in PBS-GT 6 x 60 mins and then in PBS for 30 min. For dehydration and lipid removal steps, series of increasing tetrahydrofuran (THF, Sigma-Aldrich) were used (50% THF overnight at 4°C, 80% and 3 x 100% THF for 30 min at RT). For optical clearing, slices were immersed in dibenzyl-ether (DBE, Sigma-Aldrich) for at least 15 minutes, then were kept either in DBE for storage, or covered using a glass slide with custom-made plastic supporting frame adjusted for the actual specimen thickness. The specimen was cover-slipped with DBE for the later confocal microscopic analysis.

Quantitative 3D image analysis of the interacting cholinergic and GnRH neuronal systems

For quantitative evaluation of the interacting cholinergic and GnRH neuronal systems, stacks of images were acquired with a Nikon C2 laser scanning confocal system (Nikon Instruments Europe BV, Amsterdam, Netherlands). To maximize the emitted signal intensity, sequential scanning mode was set in the software (NIS Elements AR, Nikon). For Cy3-coupled labeling, an argon laser (561 nm) and 595/40 nm emission filter (Nikon) were used. At the same time, to detect Cy5 emission, a He-Ne laser (637 nm) and a DAPI/CY5 (custom #239415 Semrock, Lake Forest, USA) dual emission filters were applied. The sampling of interacting neuronal profiles was carried out in 2 slices per mouse brain and 4 adjacent frames of each sagittal brain slice. A total of 48 imaging areas were studied in 6 brains that contained the residence of GnRH neurons (see **Fig 10**).

For quantitative analysis, 20x objective magnification (Plan-Apo VC DIC N2, NA: 0.75 WD: 1mm) was used at 1024 x 1024-pixel *x-y* image resolution. During scanning process, the pinhole diameter was set to 1

AU (Airy unit) in the acquisition software. The size of the optical thickness was 2 µm. The optical sectioning was adjusted to match pinhole size (z-step interval: 1.2 µm).

All GFP immunoreactive (IR) perikarya were counted in the z-stacks of scanned areas. GFP-IR neurons receiving VAChT-IR axonal appositions were also counted using the orthogonal view of the z-stacks. The ratio of GFP-IR neurons targeted by VAChT axons was calculated. The ratio of all GnRH-IR dendrites and those contacted VAChT-IR axons was estimated similarly. Student's t-test was used to test the significance of the differences in the morphological data and considered as significant at $p < 0.05$.

Immunoelectron microscopy

GnRH-GFP transgenic mice (No=10) were anaesthetized and perfused transcardially with 10 ml of 0.01 M phosphate-buffered saline (PBS), pH 7.4, followed sequentially by 30 ml fixative containing 4% acrolein and 2% paraformaldehyde (PFA) in PBS, pH 7.4, and then by 40 ml of 4% PFA in PBS, pH 7.4. The brains were removed and stored in 4% PFA in 0.1M PB overnight at 4 °C. Serial 25 µm thick, coronal sections were cut on a Leica VT 1000S vibratome (Leica Microsystems, Vienna, Austria) through medial septum-diagonal band of Broca-medial preoptic area. The sections were treated with 1% sodium borohydride in 0.1M PB for 30 minutes followed by 0.5% H_2O_2 in PBS for 15 minutes, cryoprotected in 15% sucrose in PBS for 15 min at room temperature and in 30% sucrose in PBS overnight at 4°C. The sections were incubated with 2% normal horse serum for 20 min to block the non-specific binding of antibodies. The tissue penetration of antibodies was facilitated with Photo-Flo (Kodak Photo-Flo 200 Solution) added to the used antibodies at 0.3% concentration.

The pre-treated sections were placed in a mixture of guinea pig anti-GFP serum (1:2500) and anti-VAChT serum (1:10.000) for 4 days at 4 °C. After rinsing in PBS and 0.1% cold water fish gelatin /1% bovine serum albumin (BSA) in PBS, the sections were incubated in donkey, anti-sheep IgG conjugated with 0.8 nm colloidal gold (Electron Microscopy Sciences, Fort Washington, PA) diluted at 1:100 and biotinylated anti-rabbit IgG diluted at 1:500 in PBS containing 0.1% cold water fish gelatin and 1% BSA overnight at 4°C. After washing in PBS, the sections were fixed in 1.25% glutaraldehyde in 0.1M PB for 10 min at room temperature. After further rinsing in PBS, the sections were washed in Aurion ECS buffer (Aurion, Wageningen, Netherlands) (1:10, diluted in distilled water. The sections were further rinsed in 0.2 M sodium citrate pH 7.5, and then the gold particles were silver-intensified with the Aurion R-Gent SE-LM Kit. The

sections were placed in 0.05% gold-chloride for 2x5 min at room temperature, washed in 0.2 M sodium citrate, pH 7.5, and in 3% sodium-thiosulphate solution for 10 min each at room temperature. Then the sections were treated in avidin/biotin-peroxidase complex (Vectastain Elite ABC Elite 1:500, Vector Laboratories Inc, Burlingame, US) and the GnRH-immunoreactivity was developed in 0.05% DAB /0.005% H_2O_2 in 0.05 M Tris buffer, pH 7.6.

The sections were processed for electron microscopy, first osmicated for 30 minutes (OsO_4, 1%) at room temperature, and then treated with 2% uranyl acetate in 70% ethanol for 30 min. Following dehydration in an ascending series of ethanol and propylene oxide (Sigma), the sections were flat embedded in Araldite 6005 epoxy resin (EMS) on liquid release agent coated slides and polymerized at 56 °C for 2 days. After polymerization, 60–70 nm thick ultrathin sections were cut with a Leica UCT ultramicrotome (Leica Microsystems, Wetzlar, Germany). The ultrathin sections were mounted onto Formvar-coated, single slot grids, and examined with a Hitachi H-7100 transmission electron microscope (Hitachi Ltd, Tokyo, Japan).

Cre-dependent retrograde rabies virus tract tracing

Stereotaxic surgery

A cocktail of helper viruses [pAAV-EF1a-FLEX-TVA-mCherry /pAAV-CAG-FLEX-oG-WPRE-SV40pA in a ratio of 1:1, Salk Institute, La Jolla)] was delivered by a single injection into the MS/DBB region (Bregma antero-posterior +0.85 mm, dorso-ventral -4.5 mm and medio-lateral: 0 mm) and bilateral injections into the MPA (Bregma antero-posterior +0.49 mm, dorso-ventral -5 mm and medio-lateral: ±0.25 mm) of male GnRH-Cre mice (n=15). Three weeks later bilateral injections were made with rabies ΔG-EnvA-eGFP virus (BRVenvA-2C, Charité Universitätsmedicine Berlin, Viral Core Facility) into the helper virus-infiltrated territory (Bregma antero-posterior +0.6 mm, dorso-ventral -5 mm and medio-lateral: ±0.25 mm). Due to expression of the transgenes, helper virus infected cells became red (Cre-dependent manner), while rabies virus infected cells became green (at the injection site, random manner). The starter cells expressing both transgenes became yellow (the target cells of the primary afferent cells). The helper viruses infected cells contained an upgraded version of the rabies glycoprotein (oG) that has increased the trans-synaptic labeling potential [91]. After 8-14 days of survival, mice were perfused with 4% PFA, brains were removed, and 30 μm-thick sections were cut on a freezing microtome (Reichert).

Immunohistochemical identification of rabies-infected cholinergic neurons

The fluorescent marker proteins mCherry and GFP expressed in response to the viral infections, and the cholinergic marker enzyme, Chat were detected by a triple-label immunofluorescent technique using rabbit anti-DS Red IgG (Clontech, #632496), chicken anti-GFP (Invitrogen, #A10262) and goat anti-Chat (Millipore, #AB144P) primary antibodies, and CY3, FITC and CY5 conjugated anti-rabbit (Jackson Lab, #715-165-152), anti-chicken (Jackson Lab, #703-095-155) and anti-goat (Jackson Lab, #705-165-147) secondary antibodies, respectively. Sections were mounted, cover slipped by Prolong Gold Antifade and scanned by a slide scanner (Pannoramic Scan; 3D-HISTECH, Budapest, Hungary) using 10x objective magnification. Selected sections underwent confocal analyses using a NIKON A1 confocal microscope at 20x and 60x magnification.

Immunohistochemical controls

The specificity of the used primary antisera has been reported previously. Accordingly, increasing dilutions of the primary antisera resulted in a gradual decrease and eventual disappearance of the immunostaining; omission of the primary antibodies or their pre-absorption with corresponding peptide antigens resulted in a complete loss of the immunostaining. The secondary antibodies used here were designed for multiple labeling and were preabsorbed by the manufacturer with IGs from several species, including the one in which the other primary antibody had been raised.

Real-time polymerase chain reaction (RT-PCR)

Cytoplasm sampling

GnRH cytoplasmic samples were harvested from acute forebrain slices of adult, male mice containing GnRH-GFP neurons using a patch pipette. A total of 7 samples were processed with 10 cytoplasmic fractions per sample. The tips of the glass pipettes were broken into PCR tubes, then cDNA was synthesized from the sample RNA using SuperScript IV VILO Master Mix (#11766050, Thermo Fisher Scientific, Waltham, US) according to the manufacturer's instructions.

PCR

Preamplification ran for 14 cycles (TaqMan PreAmp Master Mix Kit, Thermo Fisher Scientific, Waltham, US). Gene expression analyses were performed on a ViiA 7 real-time PCR system (Thermo Fisher

Scientific) using TaqMan assays (Thermo Fisher Scientific) according to the manufacturer's instructions for the following target genes: *Gapdh, Hprt, GnRH1, Chrm1, Chrm2, Chrm3, Chrm4, Chrm5, Chrna2, Chrna3, Chrna4, Chrna5, Chrna6, Chrna7, Chrnb1, Chrnb2, Chrnb3, Chrnb4, Chrnd, Chrne* and *Chrng*. The real-time PCR experiments were programmed to run 40 cycles. Expression of the *Gnrh* gene was detectable in all the 7 cell pools. The mean expression of *Gapdh* and *Hprt* genes in each of cytoplasmic sample pools (CPs) was used as reference (Ct_{ref}). Gene expression level (G) of the target genes was calculated as follows: $G = 2^{-\Delta Ct}$ where ΔCt is the difference in threshold cycle between the target and reference genes ($\Delta Ct = Ct_{gene} - Ct_{ref}$) [92].

Electrophysiology

Slice electrophysiology

Brain slice preparation was carried out as described earlier [57]. Briefly, after decapitation, the heads were immersed in ice-cold, low-Na cutting solution, and continuously bubbled with carbogen, a mixture of 95% O_2 and 5% CO_2; and the brains were removed rapidly from the skull. The cutting solution contained the following (in mM): saccharose 205, KCl 2.5, $NaHCO_3$ 26, $MgCl_2$ 5, NaH_2PO_4 1.25, $CaCl_2$ 1, and glucose 10. Hypothalamic blocks were dissected, and 220-µm-thick coronal slices were prepared from the mPOA with a VT-1000S vibratome (Leica Microsystems, Wetzlar, Germany) in the ice-cold, low-Na, oxygenated cutting solution. The slices containing preoptic area (POA) were transferred into artificial cerebrospinal fluid (aCSF) (in mM): NaCl 130, KCl 3.5, $NaHCO_3$ 26, $MgSO_4$ 1.2, NaH_2PO_4 1.25, $CaCl_2$ 2.5, and glucose 10, bubbled with carbogen and left for 1 h to equilibrate. Equilibration started at 33°C, and it was allowed to cool down to room temperature.

Recordings were carried out in carbogenated aCSF at 33°C. Axopatch-200B patch-clamp amplifier, Digidata-1322A data acquisition system, and pCLAMP 10.4 software (Molecular Devices Co., Silicon Valley, CA, USA) were used for recording. Neurons were visualized with a BX51WI IR-DIC microscope (Olympus Co., Tokyo, Japan). The patch electrodes (OD=1.5mm, thin wall; WPI, Worcester, MA, USA) were pulled with a Flaming-Brown P-97 puller (Sutter Instrument Co., Novato, CA, USA).

GnRH-GFP neurons were identified by brief illumination at 470 nm using an epifluorescent filter set, based on their green fluorescence, typical fusiform shape, and characteristic topography [83].

Whole cell patch clamp

Whole-cell patch-clamp measurements started with a control recording (1-5 min), then the selected receptor ligand was pipetted into the aCSF-filled measurement chamber containing the brain slice in a single bolus, and the recording continued for a further 7-10 min. Pre-treatment with extracellularly applied antagonist started 15 min before adding the ligand and the antagonist was continuously present in the aCSF during the electrophysiological recording. Each neuron served as its own control when drug effects were evaluated.

The membrane current and the mPSCs in GnRH neurons were measured as described earlier (Farkas et al., 2010). Briefly, the neurons were voltage clamped at −70 mV of holding potential. Intracellular pipette solution contained the following (in mM): HEPES 10, KCl 140, EGTA 5, $CaCl_2$ 0.1, Mg-ATP 4, and Na-GTP 0.4 (pH = 7.3 with NaOH). The resistance of the patch electrodes was 2–3 MΩ. Only cells with low holding current (10 pA) and stable baseline were used. Input resistance (R_{in}), series resistance (R_s), and membrane capacitance (C_m) were also measured before and after each treatment by using 5 mV hyperpolarizing pulses. To ensure consistent recording qualities, only cells with R_s <20 MΩ, R_{in} >500 MΩ, and C_m >10 pF was accepted. Spike-mediated transmitter release was blocked in all mPSC experiments by adding the voltage-sensitive Na-channel inhibitor tetrodotoxin (TTX; 660 nM, Tocris) to the aCSF 10 min before mPSCs were recorded. Time distribution graphs of frequencies were generated using 30 s time bins, shifted by 5 s steps, to show time courses of effect of substances.

Action potentials were recorded in whole-cell current clamp mode at 0 pA. After a control period (1-3 min), the agonists were applied, and the recording continued for 8-10 min. The antagonist pretreatments started 10 min before starting the recording. Each neuron served as its own control when drug effects were evaluated.

The intracellularly applied tetrahydrolipstatin (THL, Tocris, 10 μM) was added to the intracellular (pipette) solution. After achieving the whole-cell configuration, measurements started after 15 min. equilibration to reach a stable intracellular milieu.

Statistical significance was analyzed by Student's t-test and one-way ANOVA followed by Tukey's post-hoc test on the percentage and on the current amplitude data and considered as significant at $p < 0.05$.

Optogenetics

The applied technique has recently been published [90] with slight modification. A LED light source (CoolLED pE-100, Andover, UK, 470 nm) was fitted to the microscope, illuminating the sample via the objective lens. Whole-cell patch clamp measurements were carried out to record mPSCs in voltage-clamp or action potentials (APs) in current-clamp mode in GnRH neurons in acute brain slices of triple-transgenic, Chat-Cre-ChR2-GnRH-GFP adult male mice. The neurons were voltage clamped at a pipette holding potential −70 mV (for PSCs) and current clamped at 0 pA (for APs). The duration of a LED pulse was 5 ms. For evoked mPSCs (emPSC), LED pulses were applied at 0.2 Hz or 5 Hz (60 runs total, each run was 5 s long) and then records of the emPSC responses of the 60 runs were averaged (9 neurons from 5 mice). The ACh-R receptor antagonists mecamylamine and atropine or the $GABA_A$-R blocker picrotoxin were added to the aCSF and 10 min later the measurement was repeated.

Measurement of the firing rate or mPSCs frequency changes was carried out using LED pulses. The measurements started with a recording with no LED (for control purposes, 30 s for APs, 2 min for mPSCs) and with a subsequent LED train of 5 Hz illumination period (60 s for APs, 2 min for mPSCs). Analysis of the frequency changes was carried out on the percentage data calculated by dividing the frequency of the second period with that of the first one (control period), on 10 recorded cells from 5 animals. The ACh-R receptor antagonists mecamylamine and atropine were added to the aCSF and 10 min later the measurement was carried out in the presence of the antagonists.

Data analysis

Recordings were stored and analyzed off-line. Event detection was performed using the Clampfit module of the PClamp 10.4 software (Molecular Devices Co., Silicon Valley, CA, USA). Firing rates and mPSC frequencies were calculated as number of APs or mPSCs divided by the length of the corresponding time. Mean values of the control and treated period of the recording are calculated from these frequency values. All the experiments were self-controlled in each neuron: percentage changes in the firing rate or frequency of the mPSCs were calculated by dividing the frequency value in the treated period with that of the control period. Group data were expressed as mean ± standard error of mean (SEM). Two-tailed Student's t-test or

ANOVA was applied for comparison of groups, and the differences were considered as significant at $p < 0.05$. Detailed data of statistical analyses are in **S2-S4 Tables.**

Pharmacogenetics

Transgenic male (n=13) mice expressing mCitrine and activating (hM3Dq) designer receptors exclusively activated by designer drugs (DREADDs) (chat/cre_Δneo//GT(ROSA)26Sor_CAG/LSL_CHRM3_mCitrine (TgTm): Bl6Fx) in cholinergic neurons were used. Mice were bilaterally orchidectomized (ORX) under ketamine-xylazine anesthesia. After a week of recovery, all mice were handled and trained for tail-tip bleeding every day according to McCosh et al [93] for at least 28 days. A week before blood collection, animals were also trained every day to lick off a small bolus of low sugar containing peanut cream (~20mg) mixed with 1µl DMSO after stroking the tail [94].

After clipping the tip of the tail (1-2 mm), mice were placed on a flat surface every 3 minutes and allowed to roam freely while 3 µl of blood was collected from the tail wound. The first seven to ten blood samples were discarded to eliminate samples deriving from the after-cut period potentially affected by stress. The subsequent blood samples were immediately mixed with 57 µl of 0.1 M PBS (Invitrogen) containing 0.05% Tween 20 and 0.2% BSA (Jackson ImmunoResearch) and preserved in prediluted form in 60 µl aliquots on ice during blood collection, then stored at -20°C until LH assay. Samples for LH measurements were collected for 180 minutes which generated 60 aliquots/mouse. After collecting the 29th blood sample, animals either received vehicle (1 µl DMSO; n=6) or the DREADD ligand clozapine n-oxide (CNO, Tocris; 0.1mg/µl DMSO; 5mg/kg animal; n=7) in a single bolus of peanut cream.

Ultrasensitive luteinizing hormone (LH) measurement

The secretion pattern of luteinizing hormone (LH) secretion was monitored and measured by an extremely sensitive ELISA technique [38] developed a decade ago. In the experiment, the intra- and inter-assay coefficients of variation were 5.54 ± 2.15% and 7.62 ± 1.33 %, respectively. Overall basal levels of LH secretion were determined by combining the 10 lowest LH measurements from each mouse [95]. Mean levels of LH release were the average of all values collected over the sampling period. Basal and mean LH levels before and after administration of CNO or vehicle were determined and analyzed between treatment periods using paired t test.

Supplementary files

S1 Fig. Effect of CNO treatment on serum LH level in orchidectomized Chat-Cre-Gq DREADD mice. Diagrams show representative profiles of LH secretion in two vehicle controls (**a** and **b**) and two CNO-treated mice (**c** and **d**). Arrows show the onset of the treatments.

S2 Fig. Expression of channelrhodopsin-2 (ChR2) in cholinergic neurons of the medial septum in the Chat-Cre-ChR2 mouse. (**a**) A cluster of cholinergic neurons is immunostained for choline acetyltransferase (Chat). Some of the labeled neurons are encircled. (**b**) Immunocytochemical detection of ChR2 in Chat-cre neurons depicted in a. Note that cholinergic neurons selected in Fig. 1a also express ChR2. c. Merged image of figures a and b. The encircled neurons clearly show the co-localization of Chat and ChR2 as judged by their yellow color. The rest of the cholinergic neurons (red) also exhibit ChR2 in their cell membrane. An example (enframed) is shown at higher power in the inset. Scale bar: a, b, c: 25 μm, inset: 5 μm.

S3 Fig. Simultaneous visualization of GnRH- and channelrhodopsin-2-immunoreactive profiles in the vertical limb of the diagonal band of Broca in the Chat-Cre-ChR2-GnRH-GFP mouse. (**a**) GnRH-immunoreactive (IR) neuronal elements appear in red color, the ChR2-expressing, cholinergic profiles are green. In the center of the micrograph, a GnRH perikaryon (*asterisk*) is targeted by a ChR2-IR, cholinergic axon which establishes a somatic juxtaposition (*arrowhead*). The axosomatic contact is also confirmed in orthogonal views (**a1**: *xz* plane, **a2**: *yz* plane). Scale bar: 10 μm.

S4 Fig. Expression of Gq (hM3Dq) DREADD receptor in cholinergic neurons of the basal forebrain in the Chat-Gq (hM3Dq) DREADD mouse. (**a**) Cholinergic neurons (*red*) immunolabelled for the marker enzyme, choline acetyltransferase. (**b**) The same cholinergic neuron cluster shown in **a** is immunopositive for citrine (*green*), the reporter protein identifying the expression sites of the DREADD receptor. Note the intense labelling of both perikarya and neuronal processes. (**c**) Merged image of a and b demonstrates the total overlap of Chat and citrine immunoreactivities. The double labeled profiles appear in yellow color. Scale bar: 50 μm.

S1 Table. Primer probes used for the quantitative RT-PCR study.

S2 Table. One-way ANOVA of % changes of firing rates (for Fig.1), % changes of frequencies of mPSCs (for Fig.2), and of amplitudes of the inward currents (for Fig.4).

S3 Table. Two-tailed Student's t-test of % changes of firing rates (for Fig.2 and 6), % changes of frequencies of mPSCs (for Fig.1), and of amplitudes of inward currents (for Fig.4).

S4 Table. MPSC frequency responses upon blocking inhibitory/stimulatory muscarinic receptors and adding muscarine in the absence/presence of THL (Student's t-test and ANOVA; Fig. 5).

Acknowledgments

The authors express their gratitude to Dr. Suzanne M. Moenter (Department of Molecular and Integrative Physiology, University of Michigan, Ann Arbor, MI, USA) for the kind donation of the GnRH-GFP transgenic mice used in this study. We are also grateful to Dr. Cathrine Dulac (The Biological Labs, Harvard University, Cambridge, MA, USA) for the gift of the GnRH-Cre mouse line and to Dr. Erik Hrabovszky (Institute of Experimental Medicine, Budapest, Hungary) for critical reading of the manuscript and donation of the GnRH antibody. We appreciate the excellent technical assistance of Ms. Barbara Göblyös. Project no. RRF-2.3.1-21-2022-00011, titled National Laboratory of Translational Neuroscience has been implemented with the support provided by the Recovery and Resilience Facility of the European Union within the framework of Programme Széchenyi Plan Plus.

Funding

National Research, Development, and Innovation Office, K128278 and K142357, to ZL.

Programme Széchenyi Plan Plus, RRF-2.3.1-21-2022-00011, to ZL.

The funder had no role in the design of the study, data collection and interpretation, or the decision to submit the work for publication.

Author contributions

Csaba Vastagh, Conceptualization, Resources, Data curation, Software, Formal analysis, Investigation, Validation. Methodology, Visualization, Writing-original draft, Writing-review, and editing.

Imre Farkas, Conceptualization, Resources, Data curation, Software, Formal analysis, Investigation, Validation. Methodology, Visualization, Writing-original draft, Writing-review, and editing.

Veronika Csillag, Resources, Data curation, Software, Formal analysis, Investigation, Validation, Methodology, Visualization.

Masahiko Watanabe, Resources, Data curation, Validation, Methodology.

Imre Kalló, Conceptualization, Resources, Data curation, Software, Formal analysis, Investigation, Validation. Methodology, Visualization, Writing-original draft, Writing-review, and editing.

Zsolt Liposits, Conceptualization, Resources, Data curation, Software, Formal analysis, Funding acquisition, Investigation, Validation. Methodology, Visualization, Writing- the original draft, Project supervision, Project administration, Writing-review, and editing.

Conflict of interest

The authors declare that they have no conflict of interest with the contents of this article.

References

1. Knobil E. The neuroendocrine control of ovulation. Hum Reprod. 1988;3(4):469-72. Epub 1988/05/01. doi: 10.1093/oxfordjournals.humrep.a136730. PubMed PMID: 3292570.
2. Wray S, Grant P, Gainer H. Evidence that cells expressing luteinizing hormone-releasing hormone mRNA in the mouse are derived from progenitor cells in the olfactory placode. Proc Natl Acad Sci U S A. 1989;86(20):8132-6. Epub 1989/10/01. doi: 10.1073/pnas.86.20.8132. PubMed PMID: 2682637; PubMed Central PMCID: PMCPMC298229.
3. Liposits Z, Sétáló G, Flerkó B. Application of the silver-gold intensified 3,3'-diaminobenzidine chromogen to the light and electron microscopic detection of the luteinizing hormone-releasing hormone system of the rat brain. Neuroscience. 1984;13(2):513-25. doi: 10.1016/0306-4522(84)90245-8. PubMed PMID: 6392927.
4. Silverman AJ, Krey LC, Zimmerman EA. A comparative study of the luteinizing hormone releasing hormone (LHRH) neuronal networks in mammals. Biol Reprod. 1979;20(1):98-110. Epub 1979/02/01. doi: 10.1093/biolreprod/20.1.98. PubMed PMID: 110362.
5. Merchenthaler I, Kovacs G, Lavasz G, Setalo G. The preoptico-infundibular LH-RH tract of the rat. Brain Res. 1980;198(1):63-74. Epub 1980/09/29. doi: 10.1016/0006-8993(80)90344-3. PubMed PMID: 6996789.
6. Carmel PW, Araki S, Ferin M. Pituitary stalk portal blood collection in rhesus monkeys: evidence for pulsatile release of gonadotropin-releasing hormone (GnRH). Endocrinology. 1976;99(1):243-8. Epub 1976/07/01. doi: 10.1210/endo-99-1-243. PubMed PMID: 820547.
7. Boehm U, Zou Z, Buck LB. Feedback loops link odor and pheromone signaling with reproduction. Cell. 2005;123(4):683-95. Epub 2005/11/18. doi: 10.1016/j.cell.2005.09.027. PubMed PMID: 16290036.
8. Farkas I, Bálint F, Farkas E, Vastagh C, Fekete C, Liposits Z. Estradiol Increases Glutamate and GABA Neurotransmission into GnRH Neurons via Retrograde NO-Signaling in Proestrous Mice during the Positive Estradiol Feedback Period. eNeuro. 2018;5(4). Epub 2018/08/03. doi: 10.1523/ENEURO.0057-18.2018. PubMed PMID: 30079374; PubMed Central PMCID: PMCPMC6073979.
9. Christian CA, Moenter SM. The neurobiology of preovulatory and estradiol-induced gonadotropin-releasing hormone surges. Endocr Rev. 2010;31(4):544-77. Epub 2010/03/20. doi: 10.1210/er.2009-0023. PubMed PMID: 20237240; PubMed Central PMCID: PMCPMC3365847.
10. Farkas I, Vastagh C, Farkas E, Bálint F, Skrapits K, Hrabovszky E, et al. Glucagon-Like Peptide-1 Excites Firing and Increases GABAergic Miniature Postsynaptic Currents (mPSCs) in Gonadotropin-Releasing Hormone (GnRH) Neurons of the Male Mice via Activation of Nitric Oxide (NO) and Suppression of Endocannabinoid Signaling Pathways. Front Cell Neurosci. 2016;10:214. Epub 2016/09/12. doi: 10.3389/fncel.2016.00214. PubMed PMID: 27672360; PubMed Central PMCID: PMCPMC5018486.
11. Farkas I, Vastagh C, Sárvári M, Liposits Z. Ghrelin decreases firing activity of gonadotropin-releasing hormone (GnRH) neurons in an estrous cycle and endocannabinoid signaling dependent manner. PLoS One. 2013;8(10):e78178. Epub 2013/10/04. doi: 10.1371/journal.pone.0078178. PubMed PMID: 24124622; PubMed Central PMCID: PMCPMC3790731.
12. Balint F, Csillag V, Vastagh C, Liposits Z, Farkas I. Insulin-like growth factor 1 (IGF-1) increases GABAergic neurotransmission to GnRH neurons via suppressing the retrograde tonic endocannabinoid signaling pathway in mice. Neuroendocrinology. 2020. Epub 2020/12/29. doi: 10.1159/000514043. PubMed PMID: 33361699.
13. Csillag V, Vastagh C, Liposits Z, Farkas I. Secretin Regulates Excitatory GABAergic Neurotransmission to GnRH Neurons via Retrograde NO Signaling Pathway in Mice. Front Cell Neurosci. 2019;13:371. Epub 2019/08/23. doi: 10.3389/fncel.2019.00371. PubMed PMID: 31507377; PubMed Central PMCID: PMCPMC6716020.
14. Pitteloud N, Acierno JS, Jr., Meysing A, Eliseenkova AV, Ma J, Ibrahimi OA, et al. Mutations in fibroblast growth factor receptor 1 cause both Kallmann syndrome and normosmic idiopathic hypogonadotropic hypogonadism. Proc Natl Acad Sci U S A. 2006;103(16):6281-6. Epub 2006/04/12. doi: 10.1073/pnas.0600962103. PubMed PMID: 16606836; PubMed Central PMCID: PMCPMC1458869.
15. Pitteloud N, Zhang C, Pignatelli D, Li JD, Raivio T, Cole LW, et al. Loss-of-function mutation in the prokineticin 2 gene causes Kallmann syndrome and normosmic idiopathic hypogonadotropic

hypogonadism. Proc Natl Acad Sci U S A. 2007;104(44):17447-52. Epub 2007/10/26. doi: 10.1073/pnas.0707173104. PubMed PMID: 17959774; PubMed Central PMCID: PMCPMC2077276.
16. Iremonger KJ, Constantin S, Liu X, Herbison AE. Glutamate regulation of GnRH neuron excitability. Brain Res. 2010;1364:35-43. Epub 2010/09/03. doi: 10.1016/j.brainres.2010.08.071. PubMed PMID: 20807514.
17. DeFazio RA, Heger S, Ojeda SR, Moenter SM. Activation of A-type gamma-aminobutyric acid receptors excites gonadotropin-releasing hormone neurons. Mol Endocrinol. 2002;16(12):2872-91. Epub 2002/11/29. doi: 10.1210/me.2002-0163. PubMed PMID: 12456806.
18. Albuquerque EX, Pereira EF, Alkondon M, Rogers SW. Mammalian nicotinic acetylcholine receptors: from structure to function. Physiol Rev. 2009;89(1):73-120. Epub 2009/01/08. doi: 10.1152/physrev.00015.2008. PubMed PMID: 19126755; PubMed Central PMCID: PMCPMC2713585.
19. Caulfield MP, Birdsall NJ. International Union of Pharmacology. XVII. Classification of muscarinic acetylcholine receptors. Pharmacol Rev. 1998;50(2):279-90. Epub 1998/07/02. PubMed PMID: 9647869.
20. Blake CA, Scaramuzzi RJ, Norman RL, Kanematsu S, Sawyer CH. Nicotine delays the ovulatory surge of luteinizing hormone in the rat. Proc Soc Exp Biol Med. 1972;141(3):1014-6. Epub 1972/12/01. doi: 10.3181/00379727-141-36922. PubMed PMID: 4674930.
21. Kanematsu S, Sawyer CH. Inhibition of the progesterone-advanced LH surge at proestrus by nicotine. Proc Soc Exp Biol Med. 1973;143(4):1183-6. Epub 1973/09/01. doi: 10.3181/00379727-143-37497. PubMed PMID: 4798224.
22. Hodson CA, Davis MC, Burden HW. Effect of prior nicotine treatment on drug induced changes in serum LH concentrations in rats. Life Sci. 1997;60(25):2303-8. Epub 1997/01/01. doi: 10.1016/s0024-3205(97)00285-3. PubMed PMID: 9194685.
23. Sano A, Funabashi T, Kawaguchi M, Shinohara K, Kimura F. Intravenous injections of nicotine decrease the pulsatile secretion of LH by inhibiting the gonadotropin-releasing hormone (GnRH) pulse generator activity in female rats. Psychoneuroendocrinology. 1999;24(4):397-407. Epub 1999/05/26. doi: 10.1016/s0306-4530(98)00089-4. PubMed PMID: 10341367.
24. Fiorindo RP, Martini L. Evidence for a cholinergic component in the neuroendocrine control of luteinizing hormone (LH) secretion. Neuroendocrinology. 1975;18(4):322-32. Epub 1975/01/01. doi: 10.1159/000122413. PubMed PMID: 765884.
25. Koren D, Egozi Y, Sokolovsky M. Muscarinic involvement in the regulation of gonadotropin-releasing hormone in the cyclic rat. Mol Cell Endocrinol. 1992;90(1):87-93. Epub 1992/12/01. doi: 10.1016/0303-7207(92)90105-f. PubMed PMID: 1363791.
26. Messi E, Pimpinelli F, Andre V, Rigobello C, Gotti C, Maggi R. The alpha-7 nicotinic acetylcholine receptor is involved in a direct inhibitory effect of nicotine on GnRH release: In vitro studies. Mol Cell Endocrinol. 2018;460:209-18. Epub 2017/07/30. doi: 10.1016/j.mce.2017.07.025. PubMed PMID: 28754351.
27. Krsmanovic LZ, Mores N, Navarro CE, Saeed SA, Arora KK, Catt KJ. Muscarinic regulation of intracellular signaling and neurosecretion in gonadotropin-releasing hormone neurons. Endocrinology. 1998;139(10):4037-43. Epub 1998/09/29. doi: 10.1210/endo.139.10.6267. PubMed PMID: 9751480.
28. Todman MG, Han SK, Herbison AE. Profiling neurotransmitter receptor expression in mouse gonadotropin-releasing hormone neurons using green fluorescent protein-promoter transgenics and microarrays. Neuroscience. 2005;132(3):703-12. doi: 10.1016/j.neuroscience.2005.01.035. PubMed PMID: 15837132.
29. Varju P, Chang KC, Hrabovszky E, Merchenthaler I, Liposits Z. Temporal profile of estrogen-dependent gene expression in LHRH-producing GT1-7 cells. Neurochem Int. 2009;54(2):119-34. Epub 2008/11/25. doi: 10.1016/j.neuint.2008.11.003. PubMed PMID: 19070637.
30. Arai Y, Ishii H, Kobayashi M, Ozawa H. Subunit profiling and functional characteristics of acetylcholine receptors in GT1-7 cells. J Physiol Sci. 2017;67(2):313-23. Epub 2016/06/28. doi: 10.1007/s12576-016-0464-1. PubMed PMID: 27343174.
31. Shostak MD, Constantin S, Flannery J, Wray S. Acetylcholine regulation of GnRH neuronal activity: A circuit in the medial septum. Frontiers in Endocrinology. 2023;doi: 10.3389/fendo.2023.1147554:3-58.
32. Chu Z, Moenter SM. Endogenous activation of metabotropic glutamate receptors modulates GABAergic transmission to gonadotropin-releasing hormone neurons and alters their firing rate: a possible local feedback circuit. J Neurosci. 2005;25(24):5740-9. doi: 10.1523/JNEUROSCI.0913-05.2005. PubMed PMID: 15958740; PubMed Central PMCID: PMCPMC1201448.

33. Christian CA, Moenter SM. Estradiol induces diurnal shifts in GABA transmission to gonadotropin-releasing hormone neurons to provide a neural signal for ovulation. J Neurosci. 2007;27(8):1913-21. doi: 10.1523/JNEUROSCI.4738-06.2007. PubMed PMID: 17314287; PubMed Central PMCID: PMCPMC6673555.
34. Bhattarai JP, Park SA, Park JB, Lee SY, Herbison AE, Ryu PD, et al. Tonic extrasynaptic GABA(A) receptor currents control gonadotropin-releasing hormone neuron excitability in the mouse. Endocrinology. 2011;152(4):1551-61. Epub 20110201. doi: 10.1210/en.2010-1191. PubMed PMID: 21285326.
35. Herbison AE, Moenter SM. Depolarising and hyperpolarising actions of GABA(A) receptor activation on gonadotrophin-releasing hormone neurones: towards an emerging consensus. J Neuroendocrinol. 2011;23(7):557-69. doi: 10.1111/j.1365-2826.2011.02145.x. PubMed PMID: 21518033; PubMed Central PMCID: PMCPMC3518440.
36. Wall NR, Wickersham IR, Cetin A, De La Parra M, Callaway EM. Monosynaptic circuit tracing in vivo through Cre-dependent targeting and complementation of modified rabies virus. Proc Natl Acad Sci U S A. 2010;107(50):21848-53. Epub 20101129. doi: 10.1073/pnas.1011756107. PubMed PMID: 21115815; PubMed Central PMCID: PMCPMC3003023.
37. Roelofs TJM, Menting-Henry S, Gol LM, Speel AM, Wielenga VH, Garner KM, et al. Optimization of whole-brain rabies virus tracing technology for small cell populations. Sci Rep. 2021;11(1):10400. Epub 20210517. doi: 10.1038/s41598-021-89862-5. PubMed PMID: 34002008; PubMed Central PMCID: PMCPMC8129069.
38. Steyn FJ, Wan Y, Clarkson J, Veldhuis JD, Herbison AE, Chen C. Development of a methodology for and assessment of pulsatile luteinizing hormone secretion in juvenile and adult male mice. Endocrinology. 2013;154(12):4939-45. Epub 2013/10/03. doi: 10.1210/en.2013-1502. PubMed PMID: 24092638; PubMed Central PMCID: PMCPMC5398599.
39. Pielecka-Fortuna J, Chu Z, Moenter SM. Kisspeptin acts directly and indirectly to increase gonadotropin-releasing hormone neuron activity and its effects are modulated by estradiol. Endocrinology. 2008;149(4):1979-86. Epub 2007/12/27. doi: 10.1210/en.2007-1365. PubMed PMID: 18162521; PubMed Central PMCID: PMCPMC2276721.
40. Ordög T, Chen MD, Nishihara M, Connaughton MA, Goldsmith JR, Knobil E. On the role of gonadotropin-releasing hormone (GnRH) in the operation of the GnRH pulse generator in the rhesus monkey. Neuroendocrinology. 1997;65(5):307-13. doi: 10.1159/000127189. PubMed PMID: 9158062.
41. Zhang C, Bosch MA, Levine JE, Rønnekleiv OK, Kelly MJ. Gonadotropin-releasing hormone neurons express K(ATP) channels that are regulated by estrogen and responsive to glucose and metabolic inhibition. J Neurosci. 2007;27(38):10153-64. doi: 10.1523/JNEUROSCI.1657-07.2007. PubMed PMID: 17881521; PubMed Central PMCID: PMCPMC6672659.
42. Huang H, Xu Y, van den Pol AN. Nicotine excites hypothalamic arcuate anorexigenic proopiomelanocortin neurons and orexigenic neuropeptide Y neurons: similarities and differences. J Neurophysiol. 2011;106(3):1191-202. Epub 20110608. doi: 10.1152/jn.00740.2010. PubMed PMID: 21653710; PubMed Central PMCID: PMCPMC3174824.
43. Zhang KM, Zhao GY, Zhang BB, Xu Q, Chu CP, Jin H, et al. Nicotine enhances GABAergic inhibition of oxytocin mRNA-expressing neuron in the hypothalamic paraventricular nucleus in vitro in rats. Neurosci Lett. 2017;638:5-11. Epub 20161205. doi: 10.1016/j.neulet.2016.12.005. PubMed PMID: 27923665.
44. Richardson SB, Prasad JA, Hollander CS. Acetylcholine, melatonin, and potassium depolarization stimulate release of luteinizing hormone-releasing hormone from rat hypothalamus in vitro. Proc Natl Acad Sci U S A. 1982;79(8):2686-9. doi: 10.1073/pnas.79.8.2686. PubMed PMID: 7045869; PubMed Central PMCID: PMCPMC346266.
45. Mukai Y, Nagayama A, Itoi K, Yamanaka A. Identification of substances which regulate activity of corticotropin-releasing factor-producing neurons in the paraventricular nucleus of the hypothalamus. Sci Rep. 2020;10(1):13639. Epub 20200812. doi: 10.1038/s41598-020-70481-5. PubMed PMID: 32788592; PubMed Central PMCID: PMCPMC7424526.
46. Jeong JH, Lee DK, Jo YH. Cholinergic neurons in the dorsomedial hypothalamus regulate food intake. Mol Metab. 2017;6(3):306-12. Epub 20170112. doi: 10.1016/j.molmet.2017.01.001. PubMed PMID: 28271037; PubMed Central PMCID: PMCPMC5323886.
47. Kawai T, Abe H, Oka Y. Burst generation mediated by cholinergic input in terminal nerve-gonadotrophin releasing hormone neurones of the goldfish. J Physiol. 2013;591(22):5509-23. Epub

20130819. doi: 10.1113/jphysiol.2013.258343. PubMed PMID: 23959678; PubMed Central PMCID: PMCPMC3853492.
48. Gusev AG, Uteshev VV. Physiological concentrations of choline activate native alpha7-containing nicotinic acetylcholine receptors in the presence of PNU-120596 [1-(5-chloro-2,4-dimethoxyphenyl)-3-(5-methylisoxazol-3-yl)-urea]. J Pharmacol Exp Ther. 2010;332(2):588-98. Epub 20091118. doi: 10.1124/jpet.109.162099. PubMed PMID: 19923442; PubMed Central PMCID: PMCPMC2812114.
49. Constantin S, Shostak MD, Flannery J, Wray S. Acetylcholine regulation of GnRH neuronal activity: A circuit in the medial septum. Frontiers in Endocrinology. 2023;doi: 10.3389/fendo.2023.1147554:3-58.
50. Nakamura M, Jang IS. Muscarinic M4 receptors regulate GABAergic transmission in rat tuberomammillary nucleus neurons. Neuropharmacology. 2012;63(6):936-44. Epub 20120722. doi: 10.1016/j.neuropharm.2012.07.007. PubMed PMID: 22828639.
51. Vastagh C, Solymosi N, Farkas I, Liposits Z. Proestrus Differentially Regulates Expression of Ion Channel and Calcium Homeostasis Genes in GnRH Neurons of Mice. Front Mol Neurosci. 2019;12:137. Epub 2019/05/31. doi: 10.3389/fnmol.2019.00137. PubMed PMID: 31213979; PubMed Central PMCID: PMCPMC6554425.
52. Vastagh C, Rodolosse A, Solymosi N, Liposits Z. Altered Expression of Genes Encoding Neurotransmitter Receptors in GnRH Neurons of Proestrous Mice. Front Cell Neurosci. 2016;10:230. Epub 2016/10/07. doi: 10.3389/fncel.2016.00230. PubMed PMID: 27774052; PubMed Central PMCID: PMCPMC5054603.
53. Vastagh C, Rodolosse A, Solymosi N, Farkas I, Auer H, Sárvári M, et al. Differential Gene Expression in Gonadotropin-Releasing Hormone Neurons of Male and Metestrous Female Mice. Neuroendocrinology. 2015;102(1-2):44-59. Epub 2015/04/29. doi: 10.1159/000430818. PubMed PMID: 25925152.
54. Buls Wollman L, Fregosi RF. Chronic, Episodic Nicotine Alters Hypoglossal Motor Neuron Function at a Critical Developmental Time Point in Neonatal Rats. eNeuro. 2021;8(4). Epub 20210813. doi: 10.1523/ENEURO.0203-21.2021. PubMed PMID: 34193508; PubMed Central PMCID: PMCPMC8366915.
55. Calarco CA, Picciotto MR. Nicotinic Acetylcholine Receptor Signaling in the Hypothalamus: Mechanisms Related to Nicotine's Effects on Food Intake. Nicotine Tob Res. 2020;22(2):152-63. doi: 10.1093/ntr/ntz010. PubMed PMID: 30690485; PubMed Central PMCID: PMCPMC7297099.
56. Qin K, Dong C, Wu G, Lambert NA. Inactive-state preassembly of G(q)-coupled receptors and G(q) heterotrimers. Nat Chem Biol. 2011;7(10):740-7. Epub 20110828. doi: 10.1038/nchembio.642. PubMed PMID: 21873996; PubMed Central PMCID: PMCPMC3177959.
57. Farkas I, Kalló I, Deli L, Vida B, Hrabovszky E, Fekete C, et al. Retrograde endocannabinoid signaling reduces GABAergic synaptic transmission to gonadotropin-releasing hormone neurons. Endocrinology. 2010;151(12):5818-29. Epub 20101006. doi: 10.1210/en.2010-0638. PubMed PMID: 20926585; PubMed Central PMCID: PMCPMC3858799.
58. Bálint F, Liposits Z, Farkas I. Estrogen Receptor Beta and 2-arachidonoylglycerol Mediate the Suppressive Effects of Estradiol on Frequency of Postsynaptic Currents in Gonadotropin-Releasing Hormone Neurons of Metestrous Mice: An Acute Slice Electrophysiological Study. Front Cell Neurosci. 2016;10:77. Epub 2016/03/29. doi: 10.3389/fncel.2016.00077. PubMed PMID: 27065803; PubMed Central PMCID: PMCPMC4809870.
59. Tryon SC, Bratsch-Prince JX, Warren JW, Jones GC, McDonald AJ, Mott DD. Differential Regulation of Prelimbic and Thalamic Transmission to the Basolateral Amygdala by Acetylcholine Receptors. J Neurosci. 2023;43(5):722-35. Epub 20221219. doi: 10.1523/JNEUROSCI.2545-21.2022. PubMed PMID: 36535767; PubMed Central PMCID: PMCPMC9899087.
60. Uchigashima M, Narushima M, Fukaya M, Katona I, Kano M, Watanabe M. Subcellular arrangement of molecules for 2-arachidonoyl-glycerol-mediated retrograde signaling and its physiological contribution to synaptic modulation in the striatum. J Neurosci. 2007;27(14):3663-76. doi: 10.1523/JNEUROSCI.0448-07.2007. PubMed PMID: 17409230; PubMed Central PMCID: PMCPMC6672418.
61. Joo K, Cho KH, Youn SH, Jang HJ, Rhie DJ. Layer-specific involvement of endocannabinoid signaling in muscarinic-induced long-term depression in layer 2/3 pyramidal neurons of rat visual cortex. Brain Res. 2019;1712:124-31. Epub 20190210. doi: 10.1016/j.brainres.2019.02.007. PubMed PMID: 30753818.

62. Martin HG, Bernabeu A, Lassalle O, Bouille C, Beurrier C, Pelissier-Alicot AL, et al. Endocannabinoids Mediate Muscarinic Acetylcholine Receptor-Dependent Long-Term Depression in the Adult Medial Prefrontal Cortex. Front Cell Neurosci. 2015;9:457. Epub 20151201. doi: 10.3389/fncel.2015.00457. PubMed PMID: 26648844; PubMed Central PMCID: PMCPMC4664641.
63. Fukudome Y, Ohno-Shosaku T, Matsui M, Omori Y, Fukaya M, Tsubokawa H, et al. Two distinct classes of muscarinic action on hippocampal inhibitory synapses: M2-mediated direct suppression and M1/M3-mediated indirect suppression through endocannabinoid signalling. Eur J Neurosci. 2004;19(10):2682-92. doi: 10.1111/j.0953-816X.2004.03384.x. PubMed PMID: 15147302.
64. Campbell RE, Coolen LM, Hoffman GE, Hrabovszky E. Highlights of neuroanatomical discoveries of the mammalian gonadotropin-releasing hormone system. J Neuroendocrinol. 2022;34(5):e13115. Epub 20220503. doi: 10.1111/jne.13115. PubMed PMID: 35502534; PubMed Central PMCID: PMCPMC9232911.
65. Li X, Yu B, Sun Q, Zhang Y, Ren M, Zhang X, et al. Generation of a whole-brain atlas for the cholinergic system and mesoscopic projectome analysis of basal forebrain cholinergic neurons. Proc Natl Acad Sci U S A. 2018;115(2):415-20. Epub 20171219. doi: 10.1073/pnas.1703601115. PubMed PMID: 29259118; PubMed Central PMCID: PMCPMC5777024.
66. Wu H, Williams J, Nathans J. Complete morphologies of basal forebrain cholinergic neurons in the mouse. Elife. 2014;3:e02444. Epub 20140507. doi: 10.7554/eLife.02444. PubMed PMID: 24894464; PubMed Central PMCID: PMCPMC4038840.
67. Schäfer MK, Weihe E, Varoqui H, Eiden LE, Erickson JD. Distribution of the vesicular acetylcholine transporter (VAChT) in the central and peripheral nervous systems of the rat. J Mol Neurosci. 1994;5(1):1-26. doi: 10.1007/BF02736691. PubMed PMID: 7857778.
68. Campbell RE, Han SK, Herbison AE. Biocytin filling of adult gonadotropin-releasing hormone neurons in situ reveals extensive, spiny, dendritic processes. Endocrinology. 2005;146(3):1163-9. Epub 20041124. doi: 10.1210/en.2004-1369. PubMed PMID: 15564319.
69. Norberg R, Campbell R, Suter KJ. Ion channels and information processing in GnRH neuron dendrites. Channels (Austin). 2013;7(3):135-45. Epub 20130321. doi: 10.4161/chan.24228. PubMed PMID: 23519241; PubMed Central PMCID: PMCPMC3710340.
70. Sarter M, Parikh V, Howe WM. Phasic acetylcholine release and the volume transmission hypothesis: time to move on. Nat Rev Neurosci. 2009;10(5):383-90. doi: 10.1038/nrn2635. PubMed PMID: 19377503; PubMed Central PMCID: PMCPMC2699581.
71. Turi GF, Liposits Z, Hrabovszky E. Cholinergic afferents to gonadotropin-releasing hormone neurons of the rat. Neurochem Int. 2008;52(4-5):723-8. Epub 2007/09/08. doi: 10.1016/j.neuint.2007.09.001. PubMed PMID: 17933433.
72. Yoon H, Enquist LW, Dulac C. Olfactory inputs to hypothalamic neurons controlling reproduction and fertility. Cell. 2005;123(4):669-82. doi: 10.1016/j.cell.2005.08.039. PubMed PMID: 16290037.
73. Takács VT, Cserép C, Schlingloff D, Pósfai B, Szőnyi A, Sos KE, et al. Co-transmission of acetylcholine and GABA regulates hippocampal states. Nat Commun. 2018;9(1):2848. Epub 20180720. doi: 10.1038/s41467-018-05136-1. PubMed PMID: 30030438; PubMed Central PMCID: PMCPMC6054650.
74. Moenter SM, DeFazio RA. Endogenous gamma-aminobutyric acid can excite gonadotropin-releasing hormone neurons. Endocrinology. 2005;146(12):5374-9. Epub 20050825. doi: 10.1210/en.2005-0788. PubMed PMID: 16123153.
75. Silva MSB, Desroziers E, Hessler S, Prescott M, Coyle C, Herbison AE, et al. Activation of arcuate nucleus GABA neurons promotes luteinizing hormone secretion and reproductive dysfunction: Implications for polycystic ovary syndrome. EBioMedicine. 2019;44:582-96. Epub 20190606. doi: 10.1016/j.ebiom.2019.05.065. PubMed PMID: 31178425; PubMed Central PMCID: PMCPMC6606966.
76. Moore AM, Prescott M, Marshall CJ, Yip SH, Campbell RE. Enhancement of a robust arcuate GABAergic input to gonadotropin-releasing hormone neurons in a model of polycystic ovarian syndrome. Proc Natl Acad Sci U S A. 2015;112(2):596-601. Epub 20141230. doi: 10.1073/pnas.1415038112. PubMed PMID: 25550522; PubMed Central PMCID: PMCPMC4299257.
77. Piet R, Kalil B, McLennan T, Porteous R, Czieselsky K, Herbison AE. Dominant Neuropeptide Cotransmission in Kisspeptin-GABA Regulation of GnRH Neuron Firing Driving Ovulation. J Neurosci. 2018;38(28):6310-22. Epub 20180613. doi: 10.1523/JNEUROSCI.0658-18.2018. PubMed PMID: 29899026; PubMed Central PMCID: PMCPMC6596098.

78. Liu X, Porteous R, d'Anglemont de Tassigny X, Colledge WH, Millar R, Petersen SL, et al. Frequency-dependent recruitment of fast amino acid and slow neuropeptide neurotransmitter release controls gonadotropin-releasing hormone neuron excitability. J Neurosci. 2011;31(7):2421-30. doi: 10.1523/JNEUROSCI.5759-10.2011. PubMed PMID: 21325509; PubMed Central PMCID: PMCPMC6623676.
79. Qiu J, Nestor CC, Zhang C, Padilla SL, Palmiter RD, Kelly MJ, et al. High-frequency stimulation-induced peptide release synchronizes arcuate kisspeptin neurons and excites GnRH neurons. Elife. 2016;5. Epub 20160823. doi: 10.7554/eLife.16246. PubMed PMID: 27549338; PubMed Central PMCID: PMCPMC4995096.
80. Yip SH, Liu X, Hessler S, Cheong I, Porteous R, Herbison AE. Indirect Suppression of Pulsatile LH Secretion by CRH Neurons in the Female Mouse. Endocrinology. 2021;162(3). doi: 10.1210/endocr/bqaa237. PubMed PMID: 33543235.
81. McIntyre C, Li XF, Ivanova D, Wang J, O'Byrne KT. Hypothalamic PVN CRH neurons signal through PVN GABA neurons to suppress GnRH pulse generator frequency in female mice. Endocrinology. 2023. Epub 20230529. doi: 10.1210/endocr/bqad075. PubMed PMID: 37246581.
82. Libertun C, McCann SM. Blockade of the release of gonadotropins and prolactin by subcutaneous or intraventricular injection of atropine in male and female rats. Endocrinology. 1973;92(6):1714-24. doi: 10.1210/endo-92-6-1714. PubMed PMID: 4574978.
83. Suter KJ, Song WJ, Sampson TL, Wuarin JP, Saunders JT, Dudek FE, et al. Genetic targeting of green fluorescent protein to gonadotropin-releasing hormone neurons: characterization of whole-cell electrophysiological properties and morphology. Endocrinology. 2000;141(1):412-9. doi: 10.1210/endo.141.1.7279. PubMed PMID: 10614664.
84. Suter KJ, Wuarin JP, Smith BN, Dudek FE, Moenter SM. Whole-cell recordings from preoptic/hypothalamic slices reveal burst firing in gonadotropin-releasing hormone neurons identified with green fluorescent protein in transgenic mice. Endocrinology. 2000;141(10):3731-6. doi: 10.1210/endo.141.10.7690. PubMed PMID: 11014229.
85. Christian CA, Mobley JL, Moenter SM. Diurnal and estradiol-dependent changes in gonadotropin-releasing hormone neuron firing activity. Proc Natl Acad Sci U S A. 2005;102(43):15682-7. Epub 2005/10/17. doi: 10.1073/pnas.0504270102. PubMed PMID: 16230634; PubMed Central PMCID: PMCPMC1257388.
86. Van Keuren ML, Saunders TL. Rederivation of transgenic and gene-targeted mice by embryo transfer. Transgenic Res. 2004;13(4):363-71. doi: 10.1023/b:trag.0000040040.82536.a5. PubMed PMID: 15517995.
87. Madisen L, Mao T, Koch H, Zhuo JM, Berenyi A, Fujisawa S, et al. A toolbox of Cre-dependent optogenetic transgenic mice for light-induced activation and silencing. Nat Neurosci. 2012;15(5):793-802. Epub 2012/03/25. doi: 10.1038/nn.3078. PubMed PMID: 22446880; PubMed Central PMCID: PMCPMC3337962.
88. Armbruster BN, Li X, Pausch MH, Herlitze S, Roth BL. Evolving the lock to fit the key to create a family of G protein-coupled receptors potently activated by an inert ligand. Proc Natl Acad Sci U S A. 2007;104(12):5163-8. Epub 2007/03/02. doi: 10.1073/pnas.0700293104. PubMed PMID: 17360345; PubMed Central PMCID: PMCPMC1829280.
89. Ertürk KL, Şengül G. Three-dimensional visualization with large data sets: a simulation of spreading cortical depression in human brain. J Biomed Biotechnol. 2012;2012:352795. Epub 2012/10/31. doi: 10.1155/2012/352795. PubMed PMID: 23258956; PubMed Central PMCID: PMCPMC3509424.
90. Vastagh C, Farkas I, Scott MM, Liposits Z. Networking of glucagon-like peptide-1 axons with GnRH neurons in the basal forebrain of male mice revealed by 3DISCO-based immunocytochemistry and optogenetics. Brain Struct Funct. 2021;226(1):105-20. Epub 2020/11/09. doi: 10.1007/s00429-020-02167-7. PubMed PMID: 33169188; PubMed Central PMCID: PMCPMC7817561.
91. Kim EJ, Jacobs MW, Ito-Cole T, Callaway EM. Improved Monosynaptic Neural Circuit Tracing Using Engineered Rabies Virus Glycoproteins. Cell Rep. 2016;15(4):692-9. Epub 20160414. doi: 10.1016/j.celrep.2016.03.067. PubMed PMID: 27149846; PubMed Central PMCID: PMCPMC5063660.
92. Riedel G, Rüdrich U, Fekete-Drimusz N, Manns MP, Vondran FW, Bock M. An extended ΔCT-method facilitating normalisation with multiple reference genes suited for quantitative RT-PCR analyses of human hepatocyte-like cells. PLoS One. 2014;9(3):e93031. Epub 20140321. doi: 10.1371/journal.pone.0093031. PubMed PMID: 24658132; PubMed Central PMCID: PMCPMC3962476.

93. McCosh RB, Kreisman MJ, Breen KM. Frequent Tail-tip Blood Sampling in Mice for the Assessment of Pulsatile Luteinizing Hormone Secretion. J Vis Exp. 2018;(137). Epub 20180704. doi: 10.3791/57894. PubMed PMID: 30035764; PubMed Central PMCID: PMCPMC6102042.
94. Mamgain A, Sawyer IL, Timajo DAM, Rizwan MZ, Evans MC, Ancel CM, et al. RFamide-Related Peptide Neurons Modulate Reproductive Function and Stress Responses. J Neurosci. 2021;41(3):474-88. Epub 20201120. doi: 10.1523/JNEUROSCI.1062-20.2020. PubMed PMID: 33219002; PubMed Central PMCID: PMCPMC7821868.
95. Czieselsky K, Prescott M, Porteous R, Campos P, Clarkson J, Steyn FJ, et al. Pulse and Surge Profiles of Luteinizing Hormone Secretion in the Mouse. Endocrinology. 2016;157(12):4794-802. Epub 20161007. doi: 10.1210/en.2016-1351. PubMed PMID: 27715255.